

NONLINEAR VIBRATION ANALYSIS OF ROTORS SUPPORTED BY BALL
BEARINGS

A THESIS SUBMITTED TO
THE GRADUATE SCHOOL OF NATURAL AND APPLIED SCIENCES
OF
MIDDLE EAST TECHNICAL UNIVERSITY

BY

DOĞANCAN BAHAN

IN PARTIAL FULFILLMENT OF THE REQUIREMENTS
FOR
THE DEGREE OF MASTER OF SCIENCE
IN
MECHANICAL ENGINEERING

AUGUST 2019

Approval of the thesis:

**NONLINEAR VIBRATION ANALYSIS OF ROTORS SUPPORTED BY
BALL BEARINGS**

submitted by **DOĞANCAN BAHAN** in partial fulfillment of the requirements for the degree of **Master of Science in Mechanical Engineering Department, Middle East Technical University** by,

Prof. Dr. Halil Kalıpçılar
Dean, Graduate School of **Natural and Applied Sciences**

Prof. Dr. Sahir Arıkan
Head of Department, **Mechanical Engineering**

Prof. Dr. Ender Ciğeroğlu
Supervisor, **Mechanical Engineering, METU**

Examining Committee Members:

Assoc. Prof. Dr. Mehmet Bülent Özer
Mechanical Engineering, METU

Prof. Dr. Ender Ciğeroğlu
Mechanical Engineering, METU

Assist. Prof. Dr. Gökhan Özgen
Mechanical Engineering, METU

Assist. Prof. Dr. Ulaş Yaman
Mechanical Engineering, METU

Assoc. Prof. Dr. Can U. Doğruer
Mechanical Engineering, Hacettepe University

Date: 29.08.2019

I hereby declare that all information in this document has been obtained and presented in accordance with academic rules and ethical conduct. I also declare that, as required by these rules and conduct, I have fully cited and referenced all material and results that are not original to this work.

Name, Surname: Dođancan Bahan

Signature:

ABSTRACT

NONLINEAR VIBRATION ANALYSIS OF ROTORS SUPPORTED BY BALL BEARINGS

Bahan, Dođancan
Master of Science, Mechanical Engineering
Supervisor: Prof. Dr. Ender Ciđerođlu

August 2019, 57 pages

Performance of ball bearing-rotor systems is highly dependent on and often limited by characteristics of ball bearings. Ball bearings are nonlinear by their nature and this nonlinearity must be investigated rigorously to correctly predict vibration response of the system. The steady-state periodic response of rotor systems with nonlinear ball bearings is investigated. The rotor is modeled with the Finite Element Method. Nonlinear model for the bearings considers finite number of balls, bearing clearance and contact between balls and races. The nonlinear differential equation of motion is converted to a nonlinear algebraic equation set by Harmonic Balance Method. Receptance Method is applied to decrease the number of nonlinear equations to be solved. Newton's Method with arc-length continuation is used to solve the resulting equation set. Case studies are performed to investigate bearing vibrations such as varying compliance resonance, response to unbalance and interaction of flexible rotor-bearing vibrations.

Keywords: Rotor-bearing systems, varying compliance,

ÖZ

BİLYALI RULMANLAR İLE DESTEKLENEN ROTORLARIN LİNEER OLMAYAN TİTREŞİM ANALİZİ

Bahan, Dođancan
Yüksek Lisans, Makina Mühendisliđi
Tez Danışmanı: Prof. Dr. Ender Ciđerođlu

Ađustos 2019, 57 sayfa

Bilyalı rulman – rotor sistemlerinin performansı sıklıkla bilyalı rulman tarafından sınırlandırılmaktadır. Bilyalı rulman doğası geređi doğrusal değildir ve bu özellik sistemin frekans cevabını doğru şekilde tahmin etmek için dikkatlice incelenmelidir. Bu çalışmada doğrusal olmayan bilyalı rulmanlar ile desteklenmiş bir rotor sisteminin kararlı hal periyodik titreşimleri incelenmiştir. Rotor sistemi Sonlu Elemanlar Metodu ile modellenmiştir. Bilyalı rulman modeli sonlu sayıda topu, rulman boşluđunu ve bilya kontaklarını dikkate almaktadır. Sistemin doğrusal olmayan diferansiyel hareket denklemi Harmonik Denge Metodu ile doğrusal olmayan cebirsel denklemler setine çevrilmiştir. Reseptans metodu ile çözülecek doğrusal olmayan denklem sayısı azaltılmıştır. Çözüm yöntemi olarak yay uzunluđu sürdürme yöntemi ile Newton Metodu kullanılmıştır. Çeşitli analizler gerçekleştirilmiş ve rulmanların deđişken dirençlik rezonansı, dengesizlik yükü gibi titreşimleri ile rulman ile esnek rotor etkileşiminden kaynaklanan titreşimler incelenmiştir.

Anahtar Kelimeler: Rotor-rulman analizi, deđişken dirençlik

To my family

ACKNOWLEDGEMENTS

I want to thank my supervisor Prof. Dr. Ender Ciğeroğlu, for his supervision, guidance, and help from the beginning till the end.

I also want to express my gratitude to Mr. Bülent Acar, who introduced me to the world of rotor dynamics and taught me patiently in this intricate subject.

Another gratitude must go to the members of the Dynamic Analysis and Test Unit, without their help and sacrifice, this thesis would not have been completed.

I'm grateful to my family, who supported and encouraged me, as they always have done throughout my life.

Last thanks go to my dear friends Ersin Altın, Baran Özmen and Hasan Akman who have always been with me in my good and bad times.

TABLE OF CONTENTS

ABSTRACT	v
ÖZ	vi
ACKNOWLEDGEMENTS	viii
TABLE OF CONTENTS	ix
CHAPTERS	
LIST OF TABLES	xi
LIST OF FIGURES	xii
LIST OF ABBREVIATIONS	xiv
LIST OF SYMBOLS	xv
1. INTRODUCTION AND LITERATURE SURVEY	1
1.1. Introduction	1
1.2. Literature Survey	5
1.3. Motivation and Scope	8
2. MATHEMATICAL MODELLING OF THE SYSTEM.....	9
2.1. Finite Element Modelling.....	9
2.1.1. Modelling of the Shaft	9
2.1.2. Modelling of the Disks	10
2.1.3. Assembling Global Matrices	11
2.2. Roller Bearing Modelling.....	11
2.2.1. Lumped-Parameter REB Model	12
3. NONLINEAR SOLUTION METHOD	15
3.1. Harmonic Balance Method.....	15

3.2. Calculation of The Fourier Coefficients of The Nonlinear Forces	19
3.3. Receptance Method.....	22
3.4. Newton’s Method with Arclength Continuation.....	24
3.5. Usage of The AFT Method for The Calculation of The Jacobian Matrix	26
3.6. Stability Analysis	28
4. VERIFICATION OF THE COMPUTER CODE	31
4.1. Verification of FE Modelling.....	31
4.2. Verification of Roller Bearing Modelling.....	33
5. CASE STUDIES	37
5.1. Effect of Asymmetry on Parametric Resonance	37
5.2. Unbalance Response Under Multiple Excitation	42
6. CONCLUSION	51
REFERENCES	53

LIST OF TABLES

TABLES

Table 4.1. Properties of the Rotor Model Used for FE Verification	32
Table 4.2. Comparison of Natural Frequencies for a Non-Rotating Shaft.....	32
Table 4.3. Parameters for JIS6306	35
Table 5.1. Position of the Disk for the Configurations for Case Study 1	37
Table 5.2. Parameters for the Shaft-Disk System for Case Study 1	37
Table 5.3. Parameters for SKF6002	43
Table 5.4. Parameters for the Shaft-Disk System for Case Study 2	43

LIST OF FIGURES

FIGURES

Figure 1.1. Main Parts of a Ball Bearing, Courtesy of SKF	1
Figure 1.2. Radial and Axial Internal Clearance in a Ball Bearing, Courtesy of SKF 2	
Figure 1.3. Schematic Hertzian Contact Ellipse for a Ball Bearing [2]	3
Figure 1.4. A typical Critical Speed Map [6]	4
Figure 1.5. Contact Status of The Balls At Different Angles During Rotation.....	5
Figure 1.6. Radial Reaction Forces of Balls During One Revolution of the Cage.....	6
Figure 1.7. Overall Reaction Force of The Bearing for One Revolution of The Cage 6	
Figure 2.1. Nelson Finite Rotor Element [40]	10
Figure 2.2. Rigid and Flexible Disk Modelling [41] and Elastic Disk Modelling	10
Figure 2.3. Assembling Scheme for Global Matrices [42]	11
Figure 2.4. Sketch of the Bearing Model.....	12
Figure 2.5. Contact Angle α [24]	13
Figure 3.1. Limit Trajectory in State-Space (top) and Time Evolution [44].....	15
Figure 3.2. Iteration scheme for HBM with AFT	21
Figure 3.3. Points Per Cycle vs. Percent Error on Peaks [50]	22
Figure 3.4. Nonlinear FRF for a System with Cubic Stiffness	25
Figure 4.1. ABAQUS Model Used for Verification.....	31
Figure 4.2. Comparison of The Normalized Campbell Diagrams for 2 nd Bending Mode	33
Figure 4.3. Bearing Model in [61]	33
Figure 4.4. Comparison of Results for Vertical (Black) and Horizontal (Red) Directions for Varying Compliance Vibrations ($\delta_0 = 2 \mu m$)	34
Figure 5.1. Sketch of the System for Case Study 1	37
Figure 5.2. Total Responses for C1 (Upper) and C2 Configurations	38
Figure 5.3. Acceleration FRFs for C1 (Upper) and C2 Configurations	39

Figure 5.4. Individual Harmonic Responses for Bearing 1, C1 Top, C2 Bottom.....	40
Figure 5.5. Bearing-1 Reaction Forces for C2, $\Omega = 4389$ RPM	40
Figure 5.6. Rotor Orbits for C2 at $\Omega = 2030$ RPM Top and $\Omega = 2420$ RPM Bottom	41
Figure 5.7. Sketch of the System for Case Study 2.....	42
Figure 5.8. Relative Unbalance Angle, ψ	42
Figure 5.9. Total FRFs, Top to Bottom $\psi = 0,90,180$	44
Figure 5.10. Total Acceleration FRFs, Top to Bottom $\psi = 0,90,180$	45
Figure 5.11. Rotor Orbits for the Resonances Around 2000 and 5000 RPM, $\psi = 180$	46
Figure 5.12. Individual Harmonics for Bearing-1, Top to Bottom $\psi = 0,90,180$	47
Figure 5.13. Individual Harmonics for Bearing-2, Top to Bottom $\psi = 0,90,180$	48
Figure 5.14. Bearing-1 Reaction Forces, $\psi = 0, \Omega = 2290$ RPM	49
Figure 5.15. Bearing-2 Reaction Forces, $\psi = 180, \Omega = 3537$ RPM.....	49
Figure 5.16. Bearing-1 Reaction Forces, $\psi = 180, \Omega = 7280$ RPM.....	50

LIST OF ABBREVIATIONS

ABBREVIATIONS

AFT	Alternating Frequency Time
DOF	Degree of Freedom
EVP	Eigenvalue Problem
FE	Finite Element
DFT	Discrete Fourier Transform
FRF	Frequency Response Function
HBM	Harmonic Balance Method
NLAE	Nonlinear Algebraic Equation
ODE	Ordinary Differential Equation
REB	Roller Element Bearing
VC	Varying Compliancy

LIST OF SYMBOLS

SYMBOLS

a	Any bold lowercase letter denotes a vector
A	Any bold uppercase letter denotes a matrix
a^i	Superscript i denotes imaginary variables
a^r	Superscript r denotes real variables
a_l	Subscript l denotes linear degrees of freedom
a_n	Subscript n denotes nonlinear degrees of freedom
α	Roller contact angle
D_b	Ball diameter
D_p	Pitch diameter of the bearing
$2\delta_0$	Bearing internal clearance
E	Young's Modulus
η	Structural damping coefficient
f	Linear force vector
f_N	Nonlinear force vector
G	Gyroscopic matrix
H	Receptance matrix
J	Jacobian matrix
K	Stiffness matrix

K_H	Effective stiffness of the bearing
L	Length of the shaft
m_d	Mass of the disk
m_u	Unbalance mass
\mathbf{M}	Mass matrix
n	Number of nonlinear degrees of freedom
n_b	Stiffness exponent of rollers
N	Total degrees of freedom
N_b	Number of rollers
ν	Poisson's ratio
∇	Derivative operator in frequency domain
ψ	Relative angle between unbalance forces
r_D	Disk radius
r_i	Shaft inner radius
r_o	Shaft outer radius
ρ	Density
ω_{cage}	Cage rotational speed
ω_{VC}	Varying compliance frequency
Ω	Rotor speed
$\mathbf{Z}(\omega)$	Dynamic Stiffness Matrix
t_D	Thickness of the Disk

CHAPTER 1

INTRODUCTION AND LITERATURE SURVEY

1.1. Introduction

Bearings are indispensable parts of all rotating machines. Their durability and performance are crucial for the safety and reliability of the whole system. For this reason, many types of bearings are developed as industrial demand grows for higher performance. The most common type of bearings is fluid bearings and roller element bearings (REBs). Other types, such as magnetic bearings or gas bearings, show high potential but still have not replaced the previous two.

Although fluid bearings have almost infinite life, more load carrying capacity, higher damping, and very high-speed operability compared to REBs, their main disadvantage is their weight and space requirement. Fluid bearings need extra oil feeding systems which usually add more weight to the system than allowable. Therefore, rolling element bearings are continuing to be used extensively, especially for aerospace applications.

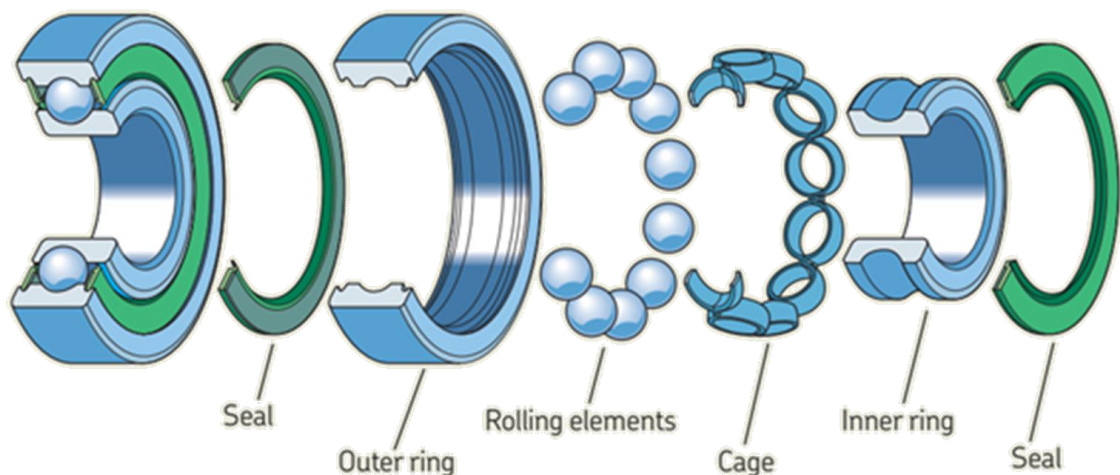


Figure 1.1. Main Parts of a Ball Bearing, Courtesy of SKF

A rolling-element bearing consists of four main parts. Inner race, which is connected to the rotating shaft, the outer race which is usually connected to a housing, rollers which roll between inner and outer races and a cage that holds the rollers together.

A rolling-element bearing would have an internal clearance, which is defined as the relative distance a ring can travel with respect to the other ring in radial or axial directions, without compressing a rolling element. This clearance is sometimes desired to compensate for thermal expansions and achieve the desired contact angle for angular contact bearings. The amount of internal clearance varies the load distribution on the rollers and directly effects the bearing life. It is desired to achieve a slightly negative clearance at operating conditions; however, this may not be possible all the time.

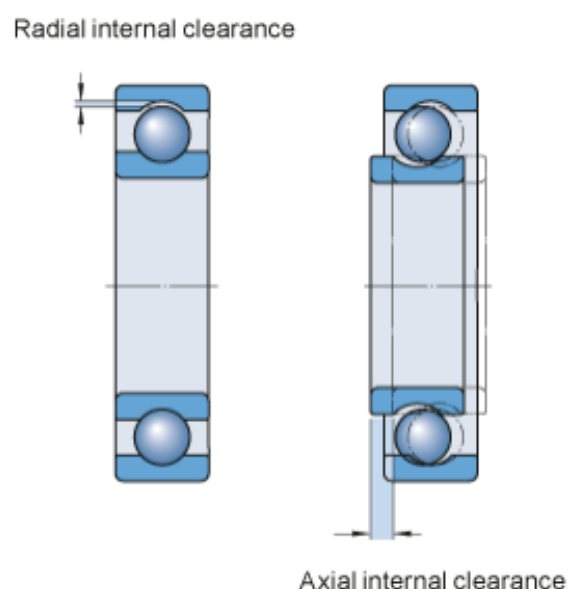


Figure 1.2. Radial and Axial Internal Clearance in a Ball Bearing, Courtesy of SKF

When contact occurs between a roller and the rings, a spherical or cylindrical body is squeezed between a concave and a convex surface. This contact is usually assumed as Hertzian type, but other approaches are also present in the literature. A recent survey might be found in [1].

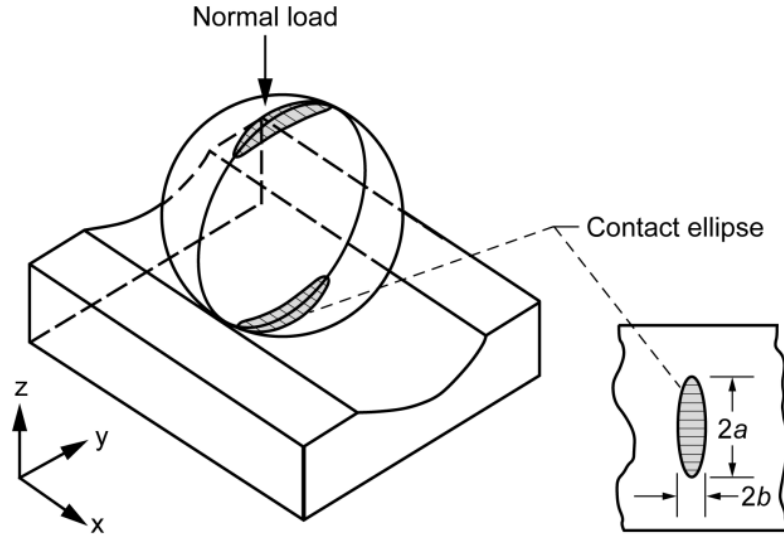


Figure 1.3. Schematic Hertzian Contact Ellipse for a Ball Bearing [2]

Both internal clearance and the contact geometry makes the nature of the bearing nonlinear. Therefore it is not an easy task to assign a linear stiffness coefficient to a particular bearing type. Gargiulo in 1980 [3], has offered simple relations, which is still used today by software such as DyRoBes [4]. Radial stiffness, K , for an angular contact radial ball bearing with this formulation is,

$$K = 0.0325 \cdot 10^6 \cdot \sqrt[3]{D_b \cdot F_r \cdot N_b^2 \cdot \cos^5(\alpha)} \quad (1.1)$$

where D_b is the ball diameter, F_r is radial force exerted on the bearing, N_b is the number of rolling elements and α is the contact angle. Note that this equation is in English engineering units. Tamura [5] has expressed linearized bearing stiffness as,

$$\begin{Bmatrix} \frac{\partial F_x}{\partial x} \\ \frac{\partial F_x}{\partial y} \end{Bmatrix} = F_r^{\frac{1}{3}} \cdot (N_b \cdot K_H)^{\frac{2}{3}} \cdot \begin{Bmatrix} 1/\Phi_1(\Psi) \\ \Phi_2(\Psi) \end{Bmatrix} \quad (1.2)$$

$$\Psi = \min \left\{ \delta_0 \cdot \left(\frac{N_b \cdot K_H}{F_r} \right)^{\frac{2}{3}}, N_b^{\frac{2}{3}} \cdot \frac{\cot^2 \left(\frac{\pi}{N_b} - 1 \right)}{2} \right\} \quad (1.3)$$

Functions Φ_1 and Φ_2 can be found in [5].

As rotors become faster and lighter, the importance of bearing stiffness to the shaft stiffness ratio on rotor dynamic behavior of the system became more evident. Classical rotor dynamics texts show this ratio on a chart called “Critical Speed Map.”

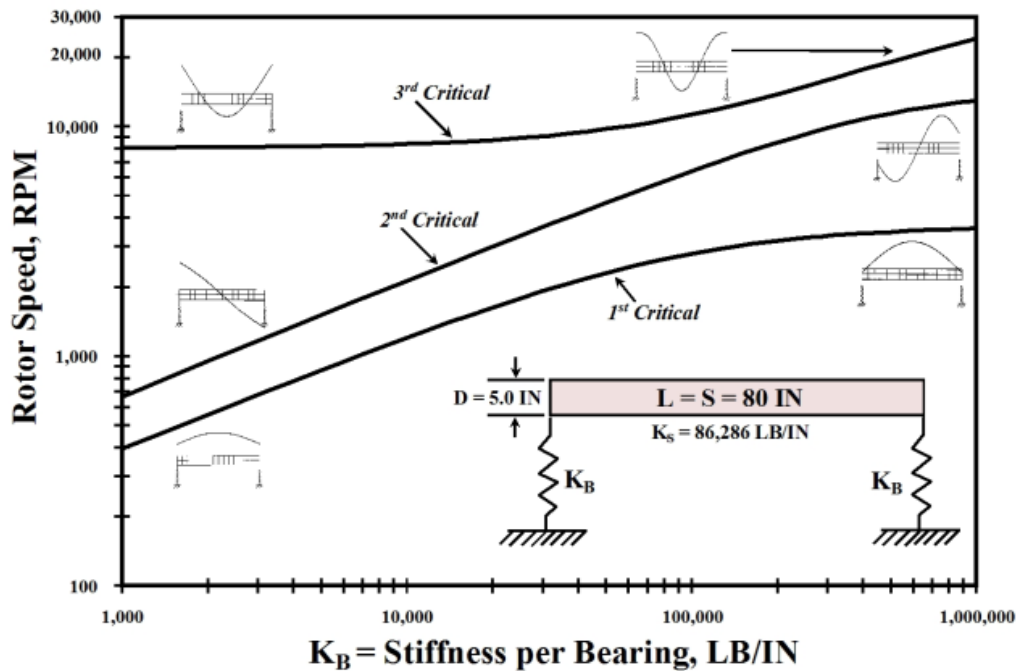


Figure 1.4. A typical Critical Speed Map [6]

In these texts, bearings are usually modeled as linear stiffness elements. However, it is seen that linear stiffness assumptions may fail to predict in-field measurements. Childs [7] has reported subsynchronous vibration in the development phase of High-Pressure Oxidizer Turbo Pump for the Space Shuttle Main Engine, originating from bearing clearances. This motion could not be observed with a linear model.

More accurate mathematical models have been developed as the need for precise analysis has increased. One difficulty encountered is, most of these models are nonlinear. Although nonlinear equation solving in the time domain is relatively straight-forward; to obtain a total dynamic picture of the system, frequency domain solutions are desired. This desire has made systems with REBs a study area of nonlinear vibration analysis.

1.2. Literature Survey

One of the first studies with nonlinear behavior of ball bearings is made by Sunnersjö [8]. In his paper, he investigated the so-called Varying Compliance vibrations. VC is an inevitable result of the REB structure. Consider a bearing with eight balls, supporting a rotating, rigid, balanced shaft. The only force the bearing carries is the weight of the shaft. As expected, weight is carried by the balls sequentially during a bearing period. During this process, the number of balls in contact varies as weight is transferred from one ball to the next one.

In Figure 1.5, the contact status of the balls for two different cage angles is presented. At the beginning of the period, i.e. $\theta_{cage} = 0^\circ$, balls number 1,2 and 8 are in contact. On the other hand, for $\theta_{cage} = 202.5^\circ$, balls number 3,4,5 and 6 are in contact. Contact intensity is shown with a colormap.

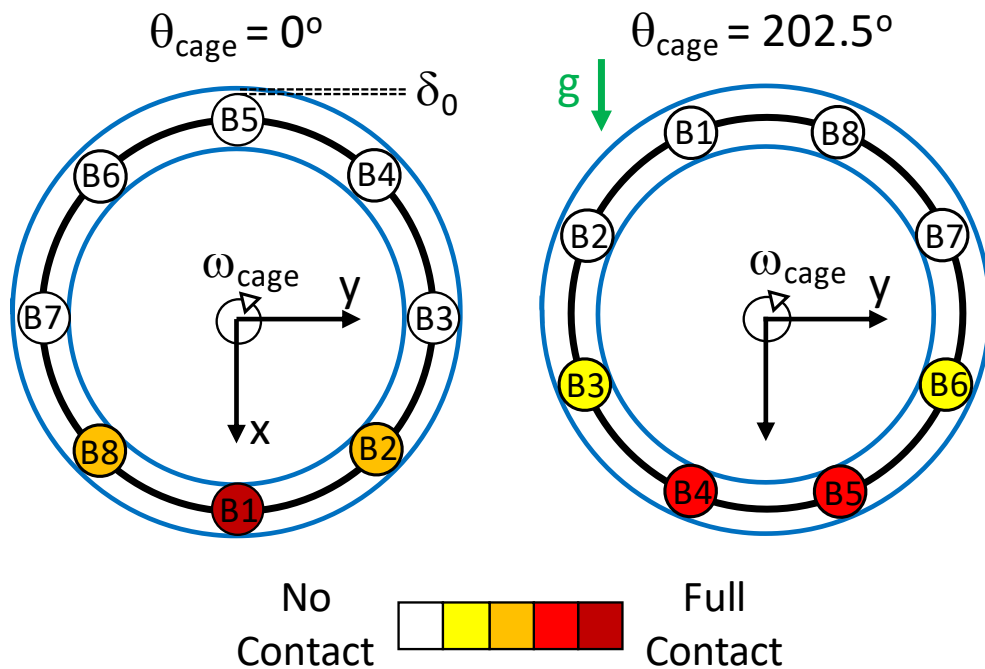


Figure 1.5. Contact Status of The Balls At Different Angles During Rotation

In Figure 1.6, the radial reaction forces of the individual rollers are shown for one revolution of the cage.

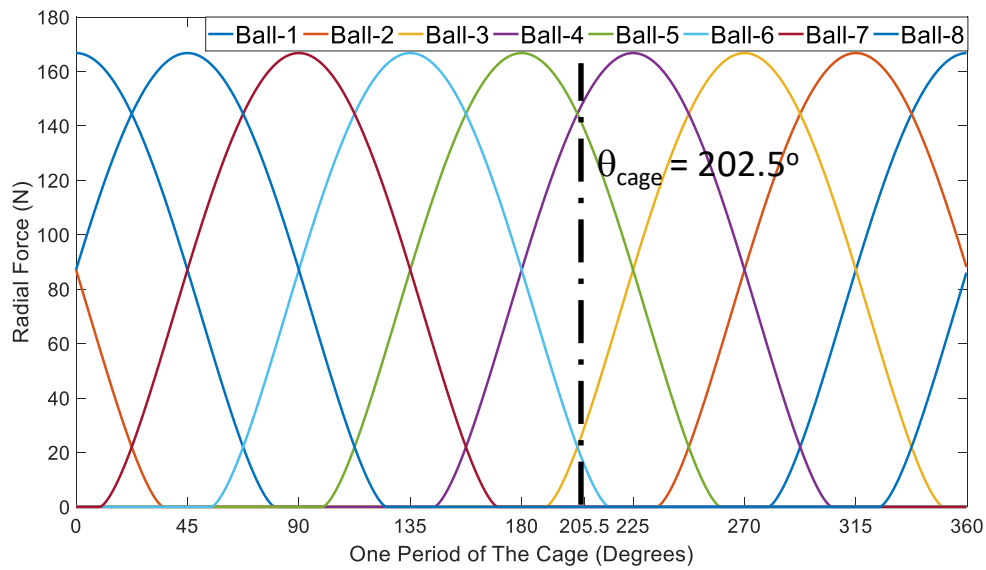


Figure 1.6. Radial Reaction Forces of Balls During One Revolution of the Cage

In Figure 1.7, the overall reaction forces of the bearing in vertical and horizontal directions are given. It is seen that reaction forces or stiffness (compliance) of the bearing is not constant but a function of time. This phenomenon is called Varying Compliance (VC). This variation is an internal source of excitation to the system even in the absence of an external time-varying one. So, any system with an REB is called parametrically excited.

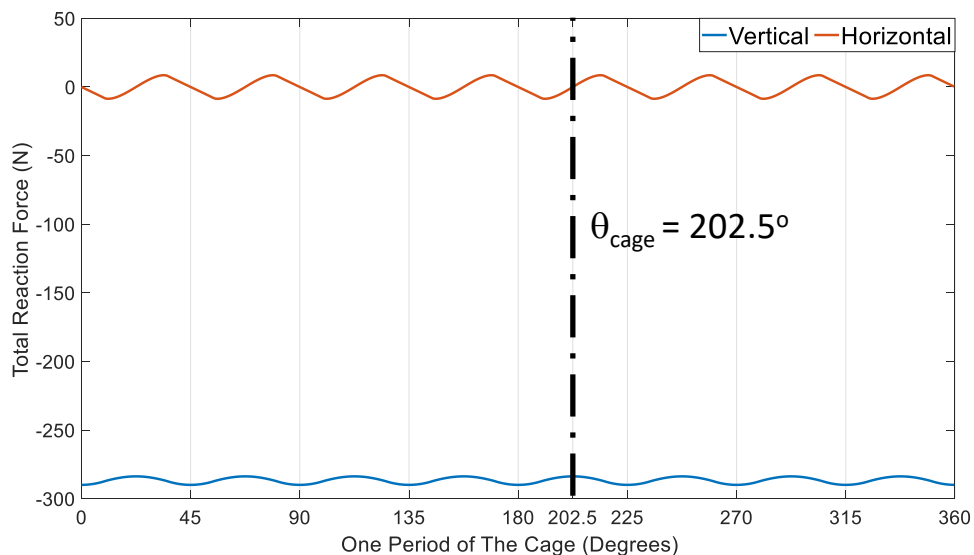


Figure 1.7. Overall Reaction Force of The Bearing for One Revolution of The Cage

In 1985, Fukata [9] had reported superharmonic, subharmonic, and chaotic vibrations for a ball bearing under constant radial load through computer simulations. In the same year, Saito [10] has analyzed the unbalance response of a Jeffcott rotor supported by bearings with clearances. He used the Harmonic Balance Method (HBM) to obtain steady-state solutions. Kim [11] also investigated a Jeffcott rotor with HBM aided by Alternating Frequency Time (AFT) scheme. The stability of the Harmonic Balance solutions is investigated by Monodromy Matrix Method. Later, Kim [12] extended his previous research to quasi-periodic response by expressing the unknowns as a double harmonic Fourier series. Ehrich [13] has investigated subcritical, superharmonic, and chaotic vibrations of a nonlinear Jeffcott rotor and compared the results with data taken from the core spool of an aircraft engine gas turbine. Mevel [14] has examined mechanisms that route to the chaotic vibration of ball bearings.

Tiwari [15–17] has studied unbalance response, the effect of radial clearance, and stability of a rigid rotor-ball bearing system both analytically and experimentally. Harsha [18,19] has analyzed effect of speed and internal clearance on stability. Lioulios [20] has considered the effect of rotational speed fluctuations on REBs. Villa [21] has considered a rotor-stator system coupled with nonlinear ball bearings. Bai [22] has examined the effect of axial preload with a 5 Degree of Freedom (DOF) flexible rotor-bearing system. Cheng [23] has considered a Jeffcott rotor with the Alford force. Bai [24] considered subharmonic resonance with a flexible 6 DOF symmetric rotor-bearing system. Zhang [25] has utilized a 5 DOF Jones-Harris type bearing model to investigate the stability of a rigid rotor-bearing system. Zhang [26] has offered a new rotor-bearing model that considers preload and varying contact angle. Hou [27] considered a dual rotor system, which has a nonlinear inter-shaft ball bearing. Wang [28] has developed a dynamic model for angular contact ball bearing-rotor systems. Jin [29] has given experimental results for a rigid rotor-ball bearing system. Yang [30] has investigated the influence of rotor eccentricity and different ball numbers on VC resonance of a Jeffcott rotor.

Up to this point, rotors are either assumed rigid or modeled with simple approximations such as a Jeffcott rotor. Nevertheless, modern rotor systems need much more detailed modeling to get results with desired precision. Villa [31] and Sinou [32] have used the Finite Element Method (FEM) to model a rotor supported by nonlinear bearings and investigated unbalance response and stability. Gupta [33] also utilized FEM and studied instability and chaos. Babu [34] has investigated an elastic rotor supported on angular contact ball bearings and concluded that flexible rotor modeling yields high amplitude vibration, especially at elevated rotor speeds, which is missed with rigid rotor approximation. Yi [35] also investigated VC resonance on a flexible rotor. Li [36] has proposed a general method which combines FEM and 6 DOF bearing models. Metsebo [37] has utilized a continuous Timoshenko beam to study unbalance response. Lu [38] investigated a dual rotor system with an inter-shaft bearing under multiple unbalance conditions.

Cao in 2018 [1], has given a review on the development of modeling of rolling bearing – rotor systems.

1.3. Motivation and Scope

It is seen in the literature that rotor-bearing systems are mostly modeled with basic rotor models. There are few studies, which use FEM [31–36,38]. Furthermore, even FEM is used, system response is investigated by varying REB parameters or unbalance masses. However, rotor – REB systems should also be studied in more detail in a rotor dynamics manner.

This thesis aimed the development of a computer code that can model a complex rotor – REB structure and analyze this system in the frequency domain. The thesis consists of mathematical modeling of rotor and bearings, nonlinear solution methodology in the frequency domain, verification of the code, and case studies.

CHAPTER 2

MATHEMATICAL MODELLING OF THE SYSTEM

2.1. Finite Element Modelling

Finite element modeling is the most widely used mathematical approach today, especially in the industry. The reason is its capabilities, such as to model any geometry without simplification, to allow multi-disciplinary calculations, i.e., thermal, structural, electrical, magnetic, acoustic and interactions between these disciplines. Modern FE solvers can now handle systems with millions of DOFs in industrially logical periods and deal with numerous nonlinearities at a time such as material nonlinearities and geometric nonlinearities.

To model shaft and disks FEM is chosen, to benefit from its flexibility to model different types of systems. This way, any shaft geometry or any number of disks or nonlinear elements, i.e., any configuration can be included in the analysis easily.

2.1.1. Modelling of the Shaft

Nelson and McVaugh [39] made one of the first attempts to include FEM in rotor dynamics modeling. They used finite beam elements to model the shaft.

A three-dimensional linear beam finite element would have twelve DOFs, six on each node on its each side. These six DOFs correspond to three displacements and three rotations. Nelson used four DOFs for the nodes by neglecting the axial and torsional flexibility of the element. A view of the element is given in Figure 2.1.

Beam finite elements can use any of the beam theories in the literature. Most of the time, Euler-Bernoulli or Timoshenko beam theories are considered. There are other ones that use higher-order beam theories to model more realistic cross-sectional shear deformations. In this thesis, the chosen element has eight DOFs and considers the

Timoshenko beam theory. The formulation of the element and resulting matrices may be found in [39].

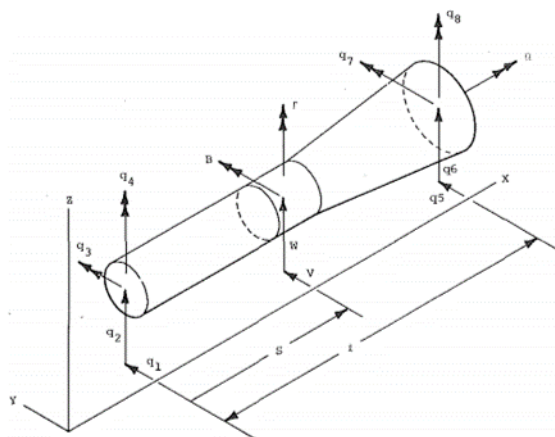


Figure 2.1. Nelson Finite Rotor Element [40]

2.1.2. Modelling of the Disks

Components such as turbine and compressor disks are usually modeled as simple disk geometries while studying shaft vibrations. The main reason for this simplification is shaft and disk vibrations are almost uncoupled, except for specific vibration modes. There are mainly three methods to include a disk in a rotor dynamic analysis. These three methods are explained in Figure 2.2. In this thesis, disks are considered as rigid and modeled as mass and inertia elements. Formulation and resulting matrices can be found in [39].

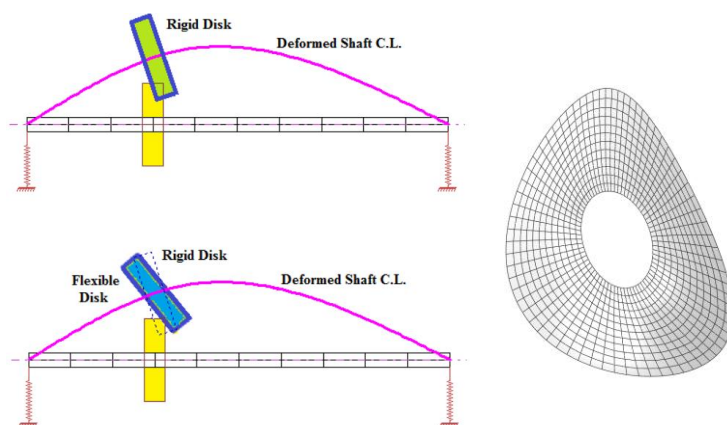


Figure 2.2. Rigid and Flexible Disk Modelling [41] and Elastic Disk Modelling

2.1.3. Assembling Global Matrices

After matrices for each element is obtained, these matrices are assembled in a particular manner to get the final global matrices of the system. The assembling process is straight forward and described in Figure 2.3.

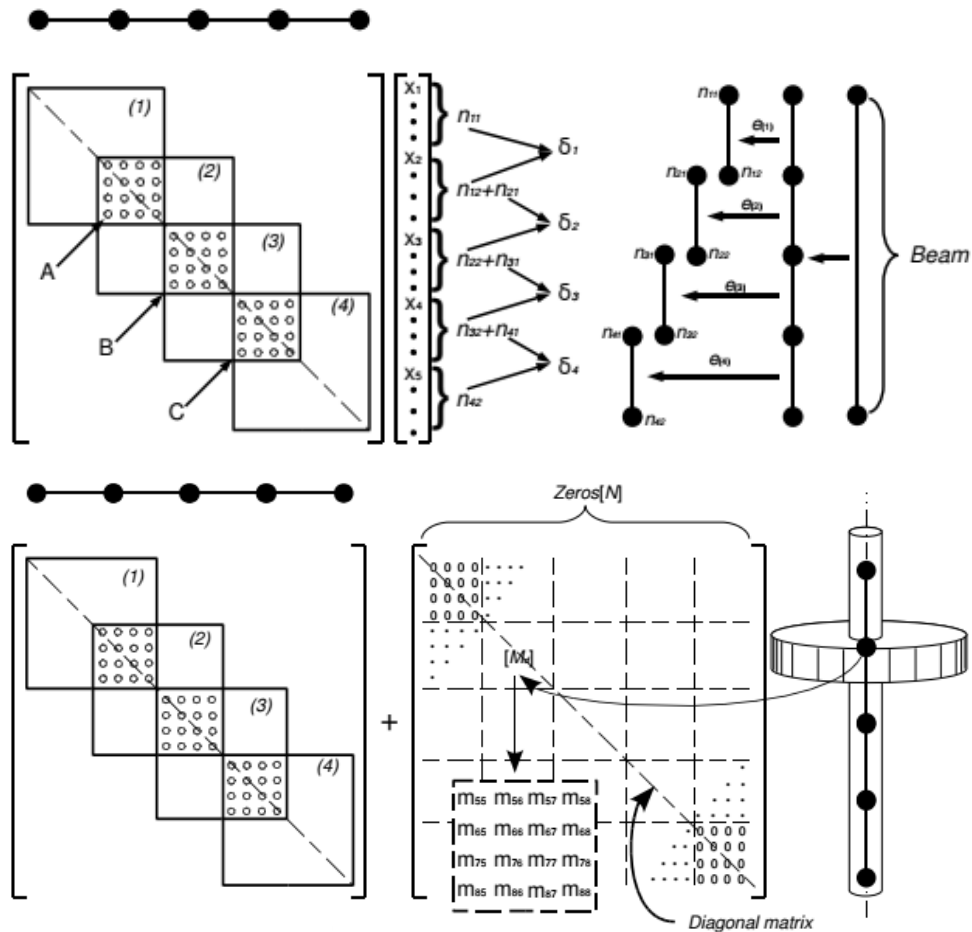


Figure 2.3. Assembling Scheme for Global Matrices [42]

2.2. Roller Bearing Modelling

Dynamic behavior of a rolling element bearing may be very complicated to predict and to model. REB modeling can be investigated under five main titles; Lumped-parameter models, quasi-static models, quasi-dynamic models, dynamic models, and lastly finite element models. A lumped parameter model is used in this thesis, so only

this model is explained below. Detailed explanations about other ones can be found in [1] and its references.

2.2.1. Lumped-Parameter REB Model

Two main assumptions of lumped-parameter models are planar bearing motion and pure rolling of bearing elements, i.e., no friction is present between element interfaces. Besides, centrifugal and gyroscopic effects are not considered, which may lead to inaccuracies, especially for high-speed systems.

Two types of lumped-parameter models are present in the literature. In the first type, each element has its own dynamic equations. In the second type, the bearing is considered as a two DOF system. The reaction force of the bearing is found by summing forces on each ball. Latter approximation is considered here. A sketch of the model is given in Figure 2.4.

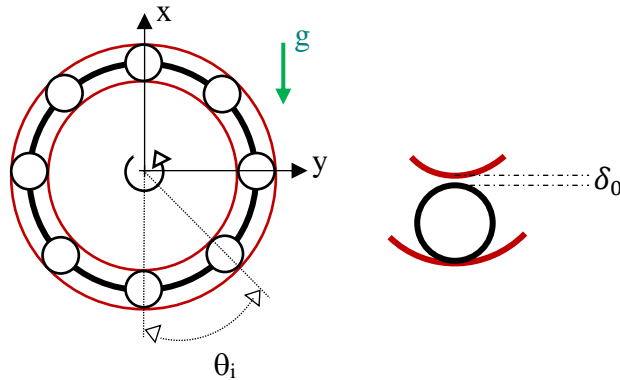


Figure 2.4. Sketch of the Bearing Model

Cage rotational speed, obtained under the assumption of no slippage of the balls can be written as follows [43],

$$\omega_{cage} = \frac{1}{2} \Omega \left(1 - \frac{D_b}{D_p} \cos(\alpha) \right) \quad (2.1)$$

where D_b and D_p are ball and pitch diameters respectively and α is the contact angle which can be calculated from,

$$\alpha = \arccos\left(1 - \frac{\delta_0}{r_{g,i} + r_{g,o} - D_b}\right) \quad (2.2)$$

where $r_{g,i}$ and $r_{g,o}$ are inner and outer groove radius respectively. Angle α is shown in Figure 2.5.

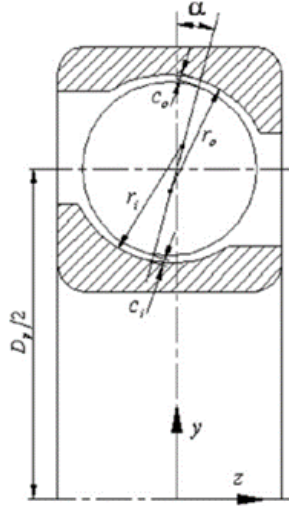


Figure 2.5. Contact Angle α [24]

In certain cases, contact angle is assumed 0° and cage speed is written as,

$$\omega_{cage} = \left(\frac{r_{b,i}}{r_{b,i} + r_{b,o}}\right)\Omega \quad (2.3)$$

Varying Compliance (VC) frequency is defined as number of balls times the cage rotation speed,

$$\omega_{VC} = N_b \cdot \omega_{cage} \quad (2.4)$$

Deflection of an individual ball can be written as follows if the inner ring is fixed to the shaft and outer ring is fixed to the ground,

$$\delta_i = \begin{cases} x \cdot \cos(\theta_i) + y \cdot \sin(\theta_i) - \delta_0 & \delta_i > 0 \\ 0 & \text{otherwise} \end{cases} \quad (2.5)$$

Where x, y are the shaft or inner ring deflections and θ_i is the angle, representing the i^{th} ball's angular position with respect to time.

$$\theta_i = (i-1) \cdot \frac{2\pi}{N_b} + \omega_{cage} \cdot t \quad (2.6)$$

The total reaction force of the bearing in x and y directions is then found by,

$$\begin{aligned} F_x &= \sum_{i=1}^{N_b} K_H \cdot \delta_i^{n_b} \cdot \cos(\theta_i) \\ F_y &= \sum_{i=1}^{N_b} K_H \cdot \delta_i^{n_b} \cdot \sin(\theta_i) \end{aligned} \quad (2.7)$$

Stiffness matrix of the bearing can be expressed by partial derivatives of its reaction forces. Such as,

$$K_B = \begin{bmatrix} \frac{\partial F_x}{\partial x} & \frac{\partial F_x}{\partial y} \\ \frac{\partial F_y}{\partial x} & \frac{\partial F_y}{\partial y} \end{bmatrix} \quad (2.8)$$

and,

$$\begin{aligned} \frac{\partial F_x}{\partial x} &= \sum_{i=1}^{N_b} K_H \cdot n_b \cdot \delta_i^{(n_b-1)} \cdot \cos^2(\theta_i) \\ \frac{\partial F_y}{\partial y} &= \sum_{i=1}^{N_b} K_H \cdot n_b \cdot \delta_i^{(n_b-1)} \cdot \sin^2(\theta_i) \\ \frac{\partial F_x}{\partial y} &= \frac{\partial F_y}{\partial x} = \sum_{i=1}^{N_b} K_H \cdot n_b \cdot \delta_i^{(n_b-1)} \cdot \cos(\theta_i) \cdot \sin(\theta_i) \end{aligned} \quad (2.9)$$

CHAPTER 3

NONLINEAR SOLUTION METHOD

Long-term behavior of nonlinear dynamic systems can be classified into four categories; Stationary, periodic, quasi-periodic, and chaotic (erratic). The time evolution of these systems and their state-space trajectories are given in Figure 3.1.

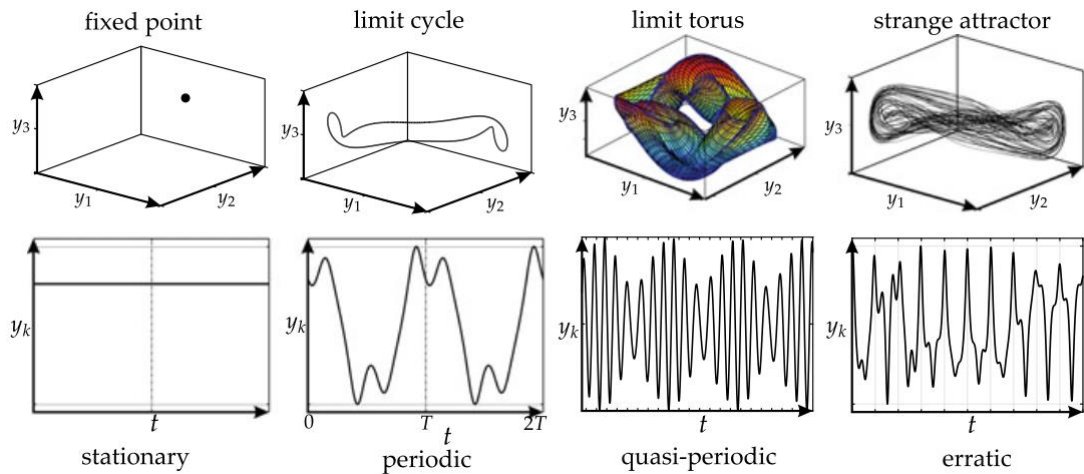


Figure 3.1. Limit Trajectory in State-Space (top) and Time Evolution [44]

The last three of these cases are observed both analytically and experimentally for REB-rotor structures.

3.1. Harmonic Balance Method

The name Harmonic Balance Method (HBM) came out in 1936. However, it has been started to be used widely only since the sixties, in the fields of mechanical and electrical engineering [45]. Today, it has become a well-known approach to analyze a nonlinear vibratory system in the frequency domain, i.e., to find the steady-state response.

HBM is focused on periodic responses of systems, the second case in Figure 3.1. HBM for quasi-periodic responses is an active research area, but it is out of scope for this thesis [46–48].

Any periodic signal can be written as a Fourier series expansion as follows,

$$y(t) = y_0 + \sum_{p=1}^{\infty} (y_{c,p} \cdot \cos(p \cdot \omega \cdot t) + y_{s,p} \cdot \sin(p \cdot \omega \cdot t)) \quad (3.1)$$

Here, $y_{c,p}$ and $y_{s,p}$ are the cosine and sine coefficients for the p^{th} harmonic respectively. ω is called the base frequency which determines the period and all other frequencies present in the series are integer number multiples of this base frequency. Recall that this is necessary for periodicity.

HBM is originated from the idea that, if the nonlinear system is excited periodically, its answer will also be periodic. Therefore, both the excitation and the response can be expressed as a Fourier series. Of course, a Fourier series will have infinite terms; however, practice shows us after using a certain number of terms, the truncation of upper ones will result in insignificant errors, especially for engineering purposes. Most of the time, a “number of harmonics to be used” convergence study is done, similar to a mesh convergence study in FE analysis.

The main objective of the method is to transform the set of nonlinear Ordinary Differential Equations (ODEs) into a set of nonlinear algebraic equations (NLAEs). After expressing each term as a Fourier series expansion and inserting into the Equation of Motion (EOM), time derivatives are now transformed into *sine* and *cosine* terms. By using orthogonality property of Fourier base functions, each harmonic, i.e., each *sine* and *cosine* term, is equated in other words ‘balanced’.

One catchy but straightforward example can be the Duffing Oscillator to show the logic of HBM. Consider the nonlinear ODE,

$$m \cdot \ddot{x} + c \cdot \dot{x} + k \cdot x + k_c \cdot x^3 = f \cdot \sin(\omega \cdot t) \quad (3.2)$$

Let us assume the unknown x is periodic and can be expressed as a Fourier series expansion.

$$x(t) = x_0 + \sum_{p=1}^{N_H} (x_{c,p} \cdot \cos(p \cdot \omega \cdot t) + x_{s,p} \cdot \sin(p \cdot \omega \cdot t)) \quad (3.3)$$

where N_H is the harmonic truncation order. For this example, let $N_H = 1$ and since no static force is present, $x_0 = 0$. So,

$$\begin{aligned} x(t) &= x_{c,1} \cdot \cos(\omega \cdot t) + x_{s,1} \cdot \sin(\omega \cdot t) \\ \dot{x}(t) &= -x_{c,1} \cdot \omega \cdot \sin(\omega \cdot t) + x_{s,1} \cdot \omega \cdot \cos(\omega \cdot t) \\ \ddot{x}(t) &= -x_{c,1} \cdot \omega^2 \cdot \cos(\omega \cdot t) - x_{s,1} \cdot \omega^2 \cdot \sin(\omega \cdot t) \end{aligned} \quad (3.4)$$

The cubic nonlinear forcing $k_c \cdot x(t)^3$, after some trigonometric manipulations, can be expressed as,

$$\begin{aligned} x(t)^3 &= \frac{3}{4} \cdot (x_{c,1}^3 + x_{c,1} \cdot x_{s,1}^2) \cdot \cos(\omega \cdot t) \\ &+ \frac{3}{4} \cdot (x_{s,1}^3 + x_{c,1}^2 \cdot x_{s,1}) \cdot \sin(\omega \cdot t) \\ &+ (\dots) \cdot \cos(3 \cdot \omega \cdot t) + (\dots) \cdot \sin(3 \cdot \omega \cdot t) \end{aligned} \quad (3.5)$$

Substituting (3.4),(3.5) into (3.2) and regrouping one has,

$$\begin{aligned} &\cos(\omega t) \cdot \left\{ (k - \omega^2 m) x_{c,1} + c \omega x_{s,1} + \frac{3}{4} k_c (x_{c,1}^3 + x_{c,1} x_{s,1}^2) \right\} \\ &+ \sin(\omega t) \cdot \left\{ (k - \omega^2 m) x_{s,1} - c \omega x_{c,1} + \frac{3}{4} k_c (x_{s,1}^3 + x_{c,1}^2 x_{s,1}) \right\} \\ &+ \cos(3\omega t) \cdot \{ \dots \} + \sin(3\omega t) \cdot \{ \dots \} = F \cdot \sin(\omega t) \end{aligned} \quad (3.6)$$

Since $\cos(\omega t)$, $\sin(\omega t)$, $\cos(3\omega t)$ and $\sin(3\omega t)$ are all orthogonal Fourier base functions, to satisfy (3.6) for all t , each term must balance itself. Neglecting the higher harmonic terms written in red, one has the following two equations,

$$(k - \omega^2 m) x_{c,1} + c \omega x_{s,1} + \frac{3}{4} k_c (x_{c,1}^3 + x_{c,1} x_{s,1}^2) = 0 \quad (3.7)$$

$$(k - \omega^2 m) x_{s,1} - c \omega x_{c,1} + \frac{3}{4} k_c (x_{s,1}^3 + x_{c,1}^2 x_{s,1}) = F \quad (3.8)$$

As one can observe, the procedure started with a nonlinear ODE (3.2) and resulted in two NLAEs (3.7), (3.8). The obtained equations are functions of frequency and can be used to sweep the frequency response of the system. Instead of solving for $x(t)$, one is now solving for the coefficients of the Fourier series expansion of $x(t)$. The price to pay is the increased number of equations to be solved. HBM will result in $(2 \cdot N_H + 1) \cdot N$ equations where N is the number of unknowns in the EOM, and $+1$ accounts for the static term in (3.1).

HBM equations can be generalized for multi-DOF systems. Resulting HBM equations for the p^{th} harmonic can be written as follows,

$$\mathbf{Z}_p(\omega) \cdot \begin{Bmatrix} \mathbf{x}_{c,p} \\ \mathbf{x}_{s,p} \end{Bmatrix} + \mathbf{f}_{N,p}(\mathbf{x}) = \mathbf{f}_p \quad (3.9)$$

Where, the dynamic stiffness matrix $\mathbf{Z}_p(\omega)$ is,

$$\mathbf{Z}_p(\omega) = \begin{bmatrix} \mathbf{K} - (p \cdot \omega)^2 \mathbf{M} & (p \cdot \omega) \mathbf{D} \\ -(p \cdot \omega) \mathbf{D} & \mathbf{K} - (p \cdot \omega)^2 \mathbf{M} \end{bmatrix} \quad (3.10)$$

Whole NLAE set for the system is,

$$\mathbf{Z}(\omega) \cdot \mathbf{x} + \mathbf{f}_N(\mathbf{x}) = \mathbf{f} \quad (3.11)$$

Where,

$$\mathbf{Z}(\omega) = \text{diag}(\mathbf{Z}_0(\omega), \mathbf{Z}_1(\omega), \dots, \mathbf{Z}_p(\omega), \dots, \mathbf{Z}_{N_H}(\omega)) \quad (3.12)$$

$$\mathbf{x} = [\mathbf{x}_0^T, \mathbf{x}_{c,1}^T, \mathbf{x}_{s,1}^T, \dots, \mathbf{x}_{c,N_H}^T, \mathbf{x}_{s,N_H}^T]^T \quad (3.13)$$

$$\mathbf{f}_N = [\mathbf{f}_N^T, \mathbf{f}_{N,c,1}^T, \mathbf{f}_{N,s,1}^T, \dots, \mathbf{f}_{N,c,N_H}^T, \mathbf{f}_{N,s,N_H}^T]^T \quad (3.14)$$

$$\mathbf{f} = [\mathbf{f}_0^T, \mathbf{f}_{c,1}^T, \mathbf{f}_{s,1}^T, \dots, \mathbf{f}_{c,N_H}^T, \mathbf{f}_{s,N_H}^T]^T \quad (3.15)$$

Note that the above representation is called *cosine – sine* since *cosine* terms are written first. However, this is not obligatory. One can write the equations in *sine – cosine* representation as well. More detailed information about the theory of HBM can be found in [44].

3.2. Calculation of The Fourier Coefficients of The Nonlinear Forces

Fourier coefficients of the nonlinear forces should be expressed as functions of Fourier coefficients of nonlinear DOFs like it has been done in (3.5). Fourier integrals to determine each coefficient is given below,

$$f_{N,0} = \frac{1}{2\pi} \int_0^T f_N(t) dt \quad (3.16)$$

$$f_{N,c,p} = \frac{1}{\pi} \int_0^T f_N(t) \cdot \cos(p \cdot \omega \cdot t) dt \quad (3.17)$$

$$f_{N,s,p} = \frac{1}{\pi} \int_0^T f_N(t) \cdot \sin(p \cdot \omega \cdot t) dt \quad (3.18)$$

Above expressions are straightforward to evaluate analytically when nonlinear terms are smooth and continuous such as the cubic nonlinearity,

$$f_N(t) = k \cdot x(t)^3 \quad (3.19)$$

Let us see how fast things may get complicated when harmonic truncation order increases. Assume a displacement variable $x(t)$ with two harmonics and a bias term,

$$\begin{aligned} x(t) = & x_0 + x_{c,1} \cos(\omega \cdot t) + x_{s,1} \sin(\omega \cdot t) \\ & + x_{c,2} \cos(2 \cdot \omega \cdot t) + x_{s,2} \sin(2 \cdot \omega \cdot t) \end{aligned} \quad (3.20)$$

Let us assume nonlinear forcing will also consist of a bias term and two harmonics.

$$\begin{aligned} f_N(t) = & f_{N,0} + f_{N,c,1} \cos(\omega \cdot t) + f_{N,s,1} \sin(\omega \cdot t) \\ & + f_{N,c,2} \cos(2 \cdot \omega \cdot t) + f_{N,s,2} \sin(2 \cdot \omega \cdot t) \end{aligned} \quad (3.21)$$

For example, $f_{N,s,1}$ will be found from the following integral.

$$f_{N,s,1} = \frac{1}{\pi} \int_0^T x(t)^3 \cdot \sin(\omega \cdot t) dt \quad (3.22)$$

There are 35 terms in (3.22) according to the Multinomial Theorem, but it can be evaluated very fast with the usage of orthogonality of sines and cosines.

Now let us have a discrete nonlinearity, such as a spring with a gap. $f_N(t)$ can be stated as,

$$f_N(t) = \begin{cases} 0 & x(t) < \delta \\ k \cdot x(t) & x(t) > \delta \end{cases} \quad (3.23)$$

When trying to evaluate (3.16)-(3.18) one needs to find when $x(t)$ is greater or smaller than δ . This requires determination of the t values from the following equation in the frequency domain, since these time steps are not known apriori in most of the cases.

$$\begin{aligned} \delta = x(t) = & x_0 + x_{c,1} \cos(\omega \cdot t) + x_{s,1} \sin(\omega \cdot t) \\ & + x_{c,2} \cos(2 \cdot \omega \cdot t) + x_{s,2} \sin(2 \cdot \omega \cdot t) \end{aligned} \quad (3.24)$$

(3.24) is itself nonlinear, probably has many roots and requires nonlinear equation solving, just to find Fourier coefficients of the nonlinear forcing term. As one can observe, this method will be more cumbersome as the number of harmonics will increase. These difficulties made researchers search for more robust approaches to evaluate nonlinear forcing coefficients. Some methods, such as Incremental Harmonic Balance Method (IHBM) and Alternating Frequency Time (AFT) or different continuation schemes are proposed [45].

AFT uses Discrete Fourier Transform (DFT) and if applicable Fast Fourier Transform (FFT) techniques to switch between frequency and time domains, aiming to avoid using classical Fourier integration [49]. Estimated Fourier coefficients for the unknown vector \mathbf{x} is used to obtain the assumed periodic representation of the original unknown $x(t)$ by inverse DFT. Then, nonlinear forcing law is applied in time domain which is straight forward for nonlinearities like (3.23). Obtained time representation of the nonlinear force $f_N(t)$ is transformed into the nonlinear forcing Fourier coefficients vector \mathbf{f}_N by DFT. Iteration scheme for HBM with AFT is given in Figure 3.2

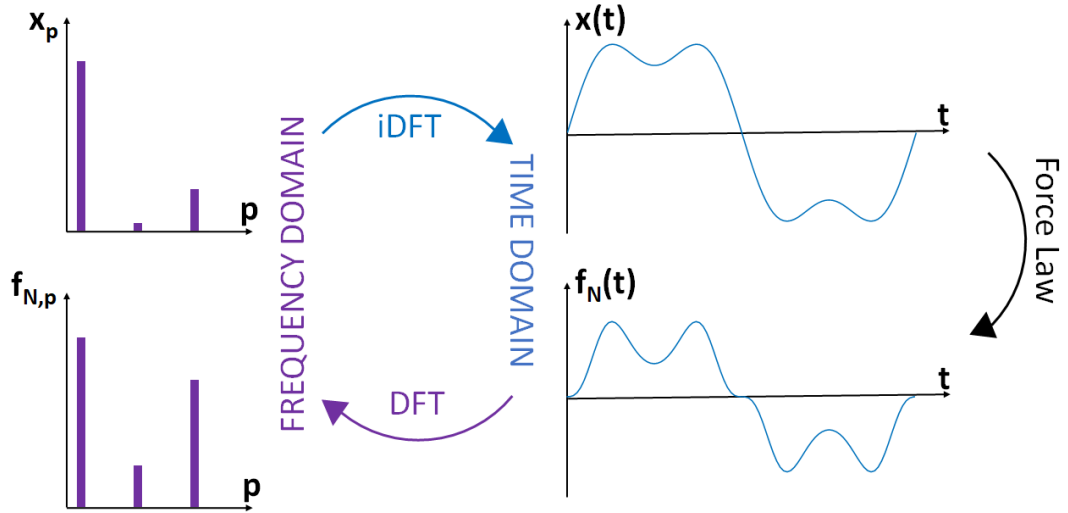


Figure 3.2. Iteration scheme for HBM with AFT

While using AFT, one should consider the basic rules of digital signal processing. Otherwise, the resulting frequency spectrum may suffer from effects like leakage, aliasing, etc. [44]. Another critical parameter is the sampling frequency. Since the exact magnitudes of the Fourier coefficients are desired, one needs to choose a higher sampling frequency than the Nyquist frequency. The relation between sampling-frequency and amplitude error is given as [50],

$$P_k = 2 \cdot \sin\left(\frac{f}{2 \cdot f_s}\right) \quad (3.25)$$

where P_k is the percentage error on peaks, f is the frequency of the sine wave and f_s is the sampling frequency. The plot of (3.25) is given in Figure 3.3, showing that ten points per cycle will give an error about 1 percent.

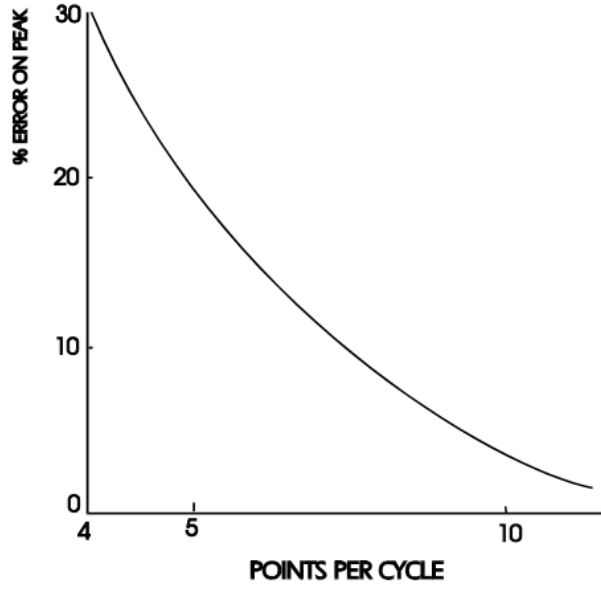


Figure 3.3. Points Per Cycle vs. Percent Error on Peaks [50]

3.3. Receptance Method

Most of the time, the number of nonlinear DOFs, i.e., DOFs connected to nonlinear elements, is much less compared to the total number of system DOFs. This difference becomes greater, especially when FEM is utilized to obtain system matrices. Therefore, researchers looked for methods to decrease the number of nonlinear equations to be solved.

Receptance Method (RM), [51–53] can be used to split linear and nonlinear DOFs and solve them separately. EOM for a rotor with nonlinear elements can be written as,

$$\mathbf{M} \cdot \ddot{\mathbf{x}}(t) + (\Omega \mathbf{G} + \mathbf{C}) \cdot \dot{\mathbf{x}}(t) + \mathbf{K}(1 + i\eta) \cdot \mathbf{x}(t) + \mathbf{f}_N(\mathbf{x}(t)) = \mathbf{f}(t) \quad (3.26)$$

Steady-state response for the p^{th} harmonic can be expressed as,

$$\mathbf{x}_p + \mathbf{H}_p \cdot (\mathbf{f}_{N,p}(\mathbf{x}) - \mathbf{f}_p) = \mathbf{0} \quad (3.27)$$

where,

$$\mathbf{H}_p = \left(\mathbf{K} \cdot (1 + i\eta) - (p \cdot \omega)^2 \cdot \mathbf{M} - i(p \cdot \omega) \cdot (\Omega \mathbf{G} + \mathbf{C}) \right)^{-1} \quad (3.28)$$

is the so-called receptance matrix. If equations are reordered such that nonlinear terms will be the bottom ones in the unknown vector, equation set can be partitioned as follows,

$$\begin{Bmatrix} \mathbf{x}_{1,p} \\ \mathbf{x}_{n,p} \end{Bmatrix} + \begin{bmatrix} \mathbf{H}_{p,ll} & \mathbf{H}_{p,ln} \\ \mathbf{H}_{p,nl} & \mathbf{H}_{p,nn} \end{bmatrix} \left(\begin{Bmatrix} \mathbf{0} \\ \mathbf{f}_{N,p}(\mathbf{x}_n) \end{Bmatrix} - \begin{Bmatrix} \mathbf{f}_{1,p} \\ \mathbf{f}_{n,p} \end{Bmatrix} \right) = \mathbf{0} \quad (3.29)$$

The second row of (3.29) is only in terms of the nonlinear DOFs and can be solved separately from the first row. This way number of nonlinear equations to be solved is decreased from $(2 \cdot N_H + 1) \cdot N$ to $(2 \cdot N_H + 1) \cdot n$. As stated, practically n is significantly less than N , so this is a considerable saving. See that after solving the second equation, $\mathbf{x}_{1,p}$ can be found directly from the first row since $\mathbf{f}_{N,p}(\mathbf{x}_n)$ will be available. Now, consider the second equation,

$$\mathbf{x}_{n,p} + \mathbf{H}_{p,nn} \cdot \mathbf{f}_{N,p}(\mathbf{x}_n) - \begin{bmatrix} \mathbf{H}_{p,nl} & \mathbf{H}_{p,nn} \end{bmatrix} \cdot \begin{Bmatrix} \mathbf{f}_{1,p} \\ \mathbf{f}_{n,p} \end{Bmatrix} = \mathbf{0} \quad (3.30)$$

All terms of (3.30) are complex, so it is a complex equation. To be solved, first, it needs to be divided into real and imaginary parts. Upon dividing and some manipulation, we have,

$$\mathbf{r}_p = \begin{Bmatrix} \mathbf{x}_{n,p}^r \\ \mathbf{x}_{n,p}^i \end{Bmatrix} + \Theta_{1,p} \begin{Bmatrix} \mathbf{f}_{N,p}^r(\mathbf{x}_n) \\ \mathbf{f}_{N,p}^i(\mathbf{x}_n) \end{Bmatrix} - \Theta_{2,p} \begin{Bmatrix} \mathbf{f}_{1,p}^r \\ \mathbf{f}_{n,p}^r \end{Bmatrix} - \Theta_{3,p} \begin{Bmatrix} \mathbf{f}_{1,p}^i \\ \mathbf{f}_{n,p}^i \end{Bmatrix} \quad (3.31)$$

where $\Theta_{1..3,p}$ stands for

$$\Theta_{1,p} = \begin{bmatrix} \mathbf{H}_{p,nn}^r & -\mathbf{H}_{p,nn}^i \\ \mathbf{H}_{p,nn}^i & \mathbf{H}_{p,nn}^r \end{bmatrix} \quad (3.32)$$

$$\Theta_{2,p} = \begin{bmatrix} \mathbf{H}_{p,nl}^r & \mathbf{H}_{p,nn}^r \\ \mathbf{H}_{p,nl}^i & \mathbf{H}_{p,nn}^i \end{bmatrix} \quad (3.33)$$

$$\Theta_{3,p} = \begin{bmatrix} -\mathbf{H}_{p,nl}^i & -\mathbf{H}_{p,nn}^i \\ \mathbf{H}_{p,nl}^r & \mathbf{H}_{p,nn}^r \end{bmatrix} \quad (3.34)$$

Note that real terms account to *cosine* representation for the unknowns and the forcing terms, whereas imaginary terms are for *sine* representation.

There are two alternatives to calculate receptance matrix. The first one is direct inversion, as shown in (3.28). The second way is using modal superposition. The latter one is computationally much cheaper for many systems however, recall that gyroscopic matrix is skew-symmetric, therefore a quadratic eigenvalue problem must be solved and complex eigenvalues and eigenvectors should be calculated for rotor systems. On top of that, the gyroscopic matrix is also frequency-dependent; therefore, the eigenvalue problem should be solved repeatedly during a frequency sweep analysis.

3.4. Newton's Method with Arclength Continuation

After application of the Receptance Method, equation set one needs to solve can be stated as,

$$\mathbf{r}(\mathbf{x}, \omega) = \left[\mathbf{r}_0^T, \mathbf{r}_1^T, \dots, \mathbf{r}_p^T, \dots, \mathbf{r}_{N_H}^T \right]^T = \mathbf{0} \quad (3.35)$$

where ω is the parameter increased or decreased incrementally to search for solutions of \mathbf{x} at those ω values. Therefore, it is frequently called a path-following or continuation parameter. Newton's method for such sets can be stated as,

$$\mathbf{x}^k = \mathbf{x}^{k-1} - \mathbf{J}(\mathbf{x}^{k-1}, \omega)^{-1} \cdot \mathbf{r}(\mathbf{x}^{k-1}, \omega) \quad (3.36)$$

where \mathbf{J} is the so-called Jacobian matrix consisting all partial derivatives of \mathbf{r} with respect to the unknown vector,

$$\mathbf{J}_{j,k} = \frac{\partial \mathbf{r}_j}{\partial \mathbf{x}_k} \quad (3.37)$$

Still, in nonlinear vibration solutions, phenomena such as bifurcations, turning points, etc. occurs.

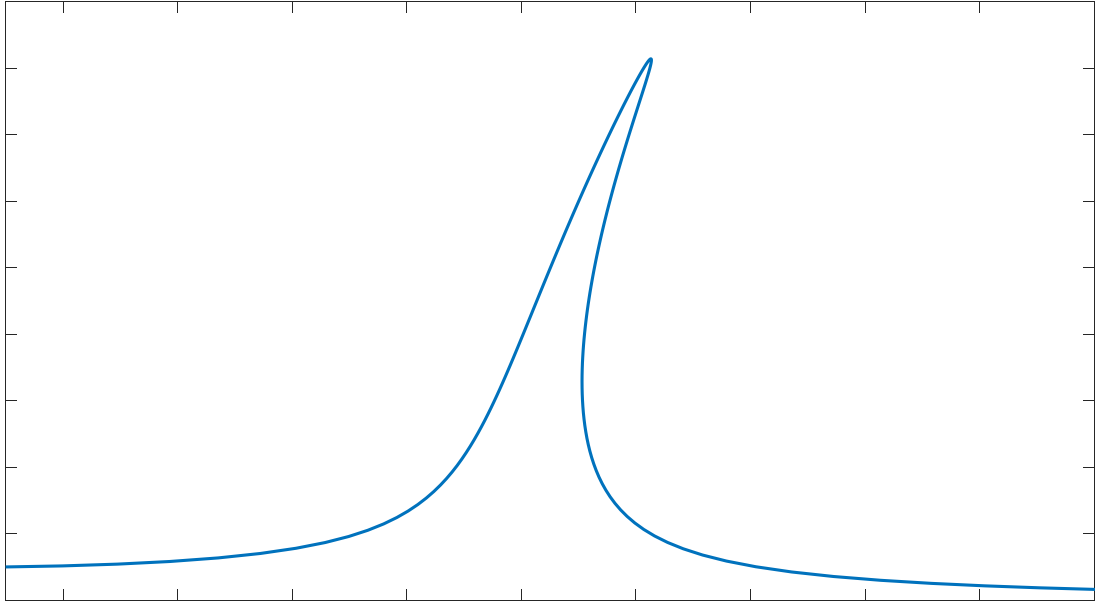


Figure 3.4. Nonlinear FRF for a System with Cubic Stiffness

As can be seen in Figure 3.4, the solution path cannot be followed by increasing or decreasing ω without knowing the turning points apriori. Moreover, the determinant of the Jacobian matrix is very small around the turning points, so it is not possible to invert it without numerical difficulties. To follow the path even at the turning points, a new parameter called the arclength parameter is introduced into the solution set. This arclength parameter, denoted by s , is the radius of a hypothetical n -dimensional sphere centered at the current solution point. The next solution point will be searched on the surface of this sphere.

$$\left(\mathbf{x}^k - \mathbf{x}^{k-1}\right)^2 + \left(\omega^k - \omega^{k-1}\right)^2 = s^2 \quad (3.38)$$

In this extended equation set the frequency term, ω , is also an unknown. Details for the iteration procedure of arclength continuation is not provided here, but can be found in [54–57].

While solving multi-harmonic problems, harmonics might differ in the order of magnitude. Also, the order of magnitude of the frequency might vary from system

vibration amplitudes. These differences can make Jacobian closer to an ill-conditioned matrix, which will cause inaccuracies during the inversion process.

To overcome this problem, a process called “Scaling” is used. Many algorithms are proposed in the literature to make the condition number of the Jacobian close to unity. For this thesis, the algorithm in [58] is used, which follows an iterative process to scale the infinity norms of both columns and rows of the Jacobian matrix to unity.

3.5. Usage of The AFT Method for The Calculation of The Jacobian Matrix

Most of the time, the calculation of the Jacobian matrix is the most time-consuming process during nonlinear equation solving. As shown in (3.37), the Jacobian matrix consists partial derivatives of the nonlinear equation set with respect to the unknowns. The fastest method to evaluate the Jacobian is to calculate these derivatives analytically. Unfortunately, this might not be possible for all nonlinearity types. Therefore, numerical differentiation schemes such as forward difference or central difference are used. This brings the necessity of many function evaluations and extends the solution time.

AFT method can help the calculation of the Jacobian by applying the chain rule. The procedure for a general case is given in [44]. Here, the procedure for the resulting equation set after the application of the Receptance Method is presented. The derivative of (3.35) respect to a variable q is as follows,

$$\begin{aligned} \frac{\partial \mathbf{r}(\mathbf{x}, \omega)}{q} = & \frac{\partial \mathbf{x}}{q} + \frac{\partial \Theta_1(\omega)}{q} \mathbf{f}_N(\mathbf{x}) + \Theta_1(\omega) \frac{\partial \mathbf{f}_N(\mathbf{x})}{q} \\ & - \frac{\partial \Theta_2(\omega)}{q} \mathbf{f}^r(\omega) - \Theta_2(\omega) \frac{\partial \mathbf{f}^r(\omega)}{q} \\ & - \frac{\partial \Theta_3(\omega)}{q} \mathbf{f}^i(\omega) - \Theta_3(\omega) \frac{\partial \mathbf{f}^i(\omega)}{q} \end{aligned} \quad (3.39)$$

If q is an element of the unknown vector \mathbf{x} :

- the first term will contain one element equal to one, and all the others are zero.

- Derivatives of $\Theta_1, \Theta_2, \Theta_3$ will be zero since they are only the functions of the frequency.
- Derivatives of the external linear forces will be zero.

Therefore, the remaining terms will be,

$$\frac{\partial \mathbf{r}(\mathbf{x}, \omega)}{q} = \frac{\partial \mathbf{x}}{q} + \Theta_1(\omega) \frac{\partial \mathbf{f}_N(\mathbf{x})}{q} \quad (3.40)$$

When AFT scheme is used, partial derivative for the nonlinear force can be expressed such as,

$$\frac{\partial \mathbf{f}_N(\mathbf{x})}{q} = \frac{\partial}{q} \left(\mathbf{T}^{-1} \cdot f_N(\mathbf{T} \cdot \mathbf{x}) \right) \quad (3.41)$$

Here \mathbf{T} and \mathbf{T}^{-1} stands for the inverse DFT and DFT operations respectively and $f_N()$ is the nonlinear force law such as in (3.23). If the differentiation is moved into the parenthesis, one has

$$\frac{\partial \mathbf{f}_N(\mathbf{x})}{q} = \mathbf{T}^{-1} \cdot \left(\mathbf{F}_N' \cdot \left(\mathbf{T} \cdot \frac{\partial \mathbf{x}}{q} \right) \right) \quad (3.42)$$

Here the matrix \mathbf{F}_N' is written as follows,

$$\mathbf{F}_N' = \text{diag} \left(f_N'(0), f_N'(t_1), f_N'(t_2), \dots, f_N'(t_{N_s-1}) \right) \quad (3.43)$$

where t_i is the i^{th} sampled time and,

$$f_N'(t_i) = \left. \frac{\partial f_N}{q} \right|_{t=t_i, x=x(t_i)} \quad (3.44)$$

as in (2.9).

It should be noted that (3.40)-(3.42) are valid only if $q \in \mathbf{x}$ and $f_N(t)$ is only a function of $x(t)$, i.e., not a function of $\dot{x}(t)$. For other cases, additional terms might appear [44].

The main benefit is that the procedure is almost independent of the number of harmonics used for the solution. So, the number of function evaluations needed for the calculation of the Jacobian matrix can be reduced significantly.

3.6. Stability Analysis

During an HB analysis, both stable and unstable solution points are obtained. What is meant by an unstable solution point is; This point mathematically exists but cannot be observed in an experiment. HB does not immediately provide information about stability; thus, further investigation is required.

The logic behind the stability analysis is to add a small perturbation to the obtained solution point and observe the time behavior of this perturbed solution. If the small perturbation dies as time evolves and the solution point goes back to its original state, it can be concluded that the solution point is stable. Otherwise, the point is unstable.

The stability of the solutions of a periodic system might be checked with Floquet Theory, by computing Floquet multipliers or exponents. The two most used methods are Monodromy Matrix Method and Hill's Method. Hill's Method is especially suitable for the Harmonic Balance process since it uses the Fourier Coefficients of the obtained solution. With Hill's Method, Floquet exponents are calculated by the quadratic eigenvalue problem (EVP) in (3.45).

$$\Delta_2 \cdot \lambda^2 + \Delta_1 \cdot \lambda + \mathbf{J} = \mathbf{0} \quad (3.45)$$

where $\Delta_{1,2}$ is given as follows,

$$\Delta_1 = 2 \cdot \omega \cdot \nabla \cdot \otimes \cdot \mathbf{M} + \mathbf{I}_{(2N_H+1)} \otimes \mathbf{D} \quad (3.46)$$

$$\Delta_2 = \mathbf{I}_{(2N_H+1)} \otimes \mathbf{M} \quad (3.47)$$

where \otimes is the Kronecker delta product, ∇ is the derivative operator in the frequency domain [59], \mathbf{J} is the Jacobian matrix in (3.37), \mathbf{I} is the identity matrix of size $(2N_H + 1)$ and \mathbf{D} is the coefficient of the velocity term in the equation of motion, i.e. $(\mathbf{C} + \mathbf{G})$ in (3.26).

The procedure to obtain this EVP from a perturbed solution point is not given here but can be found in [60]. Derivative operator in the frequency domain, ∇ , is expressed as,

$$\nabla = \text{diag}(\mathbf{0}, \nabla_1, \dots, \nabla_p, \dots, \nabla_{N_H}) \quad (3.48)$$

where ∇_p for *cosine – sine* representation is,

$$\nabla_p = p \begin{bmatrix} 0 & 1 \\ -1 & 0 \end{bmatrix} \quad (3.49)$$

for *sine – cosine* representation, -1 and 1 terms should be switched. The representation of ∇ and procedure followed to obtain the Jacobian matrix should be consistent.

$\Delta_{1,2}$ matrices in (3.46), for *cosine – sine* representation, can be written explicitly as,

$$\Delta_1 = \text{diag} \left(\mathbf{D}, \begin{bmatrix} \mathbf{D} & 2\omega\mathbf{M} \\ -2\omega\mathbf{M} & \mathbf{D} \end{bmatrix}, \dots, \begin{bmatrix} \mathbf{D} & 2N_H\omega\mathbf{M} \\ -2N_H\omega\mathbf{M} & \mathbf{D} \end{bmatrix} \right) \quad (3.50)$$

$$\Delta_2 = \text{diag}(\mathbf{M}, \mathbf{M}, \dots, \mathbf{M}) \quad (3.51)$$

One should note when Receptance Method is utilized, the Jacobian Matrix obtained is not consistent with the formulation in (3.45). One should reformulate the EVP or multiply the Jacobian with the Dynamic Stiffness Matrix, (3.12), to overcome the problem.

Floquet exponents or multipliers will also provide information about what kind of stability loss has occurred. For a stable solution point, all Floquet multipliers must lie within a unit circle in the complex plane. The multipliers may leave the unit circle in three ways, and each way addresses a different kind of stability loss [59,61].

- When a multiplier goes beyond +1, trans-critical, symmetry-breaking or cyclic-fold bifurcations may occur. Cyclic fold bifurcation indicates that the system has jumped from a periodic solution point to another periodic solution point.

- When a multiplier goes beyond -1, period-doubling bifurcation occurs, meaning that the period of the solution is doubled.
- If two complex conjugate multipliers leave the circle, secondary Hopf or Neimark-Sacker bifurcation occurs, indicating transition from periodic to aperiodic response.

The relation between a Floquet multiplier and exponent is,

$$\mu = e^{\lambda T} \quad (3.52)$$

where μ is the multiplier for the corresponding exponent λ from (3.45) and T is the solution period.

One major drawback of Hill's Method is the quality of the eigenvalues calculated. The size of the eigenvalue problem in (3.45) should be $\infty \cdot \infty$ with the original formulation [60]. However, due to the truncation of harmonics as mentioned in Section 3.1, EVP becomes finite, and some eigenvalues become less accurate than the others. The size of the EVP in (3.45) is $(2N_H + 1) \cdot N$. Floquet Theory needs N multipliers to decide on stability so eigenvalues should be filtered to choose the most accurate N ones from the total $(2N_H + 1) \cdot N$.

There are two methods for this elimination in the literature. The first one states that eigenvalues with the smallest imaginary part should be selected [59]. The second one uses eigenvalues, which has the most "symmetric" eigenvectors [60]. Till today, there is no consensus about which method should be followed [44].

CHAPTER 4

VERIFICATION OF THE COMPUTER CODE

Computer code developed during the thesis can be divided into three sections. These are:

1. Generation of system matrices with FEM
2. Nonlinear forcing calculation for roller bearing model
3. Nonlinear solver which uses HBM with AFT and Newton's method with arclength continuation

First, system matrices are verified with commercial FE program ABAQUS. Later, the second and third sections are verified with the literature data.

4.1. Verification of FE Modelling

A shaft model with disks is used for verification. The model can be seen in Figure 4.1



Figure 4.1. ABAQUS Model Used for Verification

The model consists of 20 equal length B32 quadratic beam elements that use the Timoshenko beam theory. The beam section uses the thick-walled formulation. Axial and torsional DOFs of the nodes are constrained. At two locations, mass and inertia elements are added to the shaft to simulate two disks. The properties of the system are given in Table 4.1.

Table 4.1. Properties of the Rotor Model Used for FE Verification

Shaft Inner Radius	5 mm	Disk 1 Location	100 mm from left end
Shaft Outer Radius	10 mm	Disk 2 Location	300 mm from left end
Shaft Length	500 mm	Disk Inner Radius	5 mm
Young's Modulus	70 GPa	Disk Outer Radius	30 mm
Density	2300 kg/m ³	Disk Thickness	5mm
Poisson's Ratio	0.3		

Model is constrained to the ground at two ends. The first ten natural frequency results for a non-rotating shaft are given in Table 4.2.

Table 4.2. Comparison of Natural Frequencies for a Non-Rotating Shaft

Mode	ABAQUS (Hz)	CODE (Hz)	% Error
1 st Bending	384.3	383.9	0.12
1 st Bending	384.3	383.9	0.12
2 nd Bending	1032.2	1029.7	0.25
2 nd Bending	1032.2	1029.7	0.25
3 rd Bending	2021.1	2013.9	0.36
3 rd Bending	2021.1	2013.9	0.36
4 th Bending	3164.8	3149.9	0.47
4 th Bending	3164.8	3149.9	0.47
5 th Bending	4964.8	4945.7	0.38
5 th Bending	4964.8	4945.7	0.38

Later, to include and verify gyroscopic effects a normalized Campbell diagram is drawn and compared for the second bending mode. From Figure 4.2, it can be observed that curves are parallel to each other, meaning that gyroscopic effects are modeled correctly.

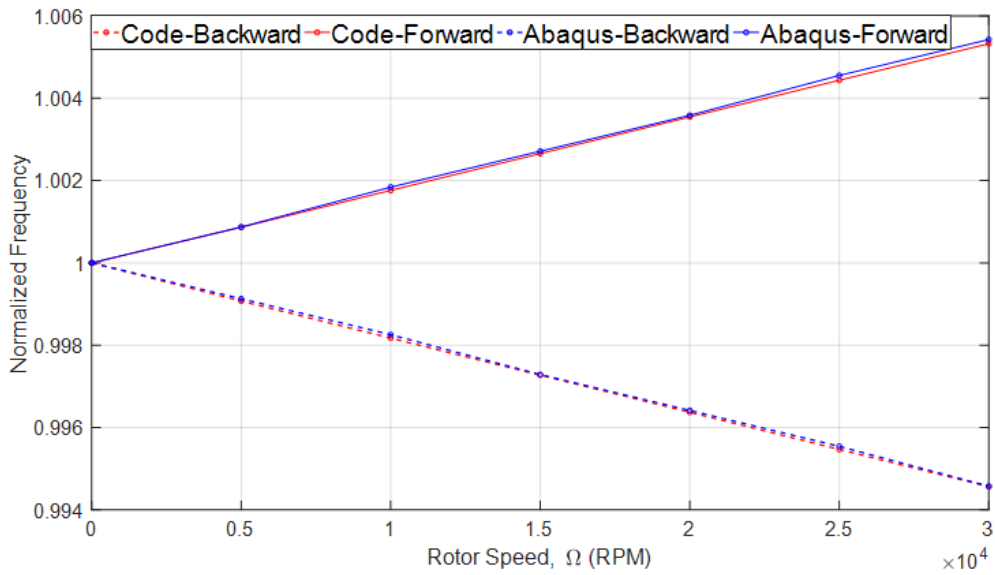


Figure 4.2. Comparison of The Normalized Campbell Diagrams for 2nd Bending Mode

4.2. Verification of Roller Bearing Modelling

To verify the lumped parameter roller bearing model explained in Section 2.2.1, a model consisting of a single bearing is chosen from the literature [61]. This paper investigates primary parametric resonances of a lumped-parameter ball bearing. A sketch of the model is given in Figure 4.3 and the equation of motion for the bearing can be found in (4.1).

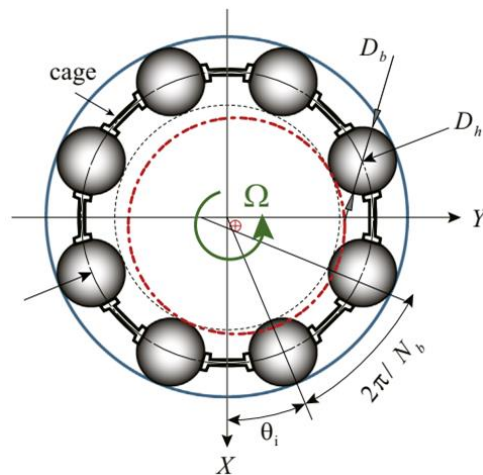


Figure 4.3. Bearing Model in [61]

$$m \cdot \begin{Bmatrix} \ddot{x} \\ \ddot{y} \end{Bmatrix} + c \cdot \begin{Bmatrix} \dot{x} \\ \dot{y} \end{Bmatrix} + \begin{Bmatrix} F_x \\ F_y \end{Bmatrix} = \begin{Bmatrix} W \\ 0 \end{Bmatrix} \quad (4.1)$$

Where, F_x and F_y stands for nonlinear bearing forces and W is the weight of the bearing. The bearing type used for the analysis is JIS6306 and all parameters can be found in Table 4.3. A comparison of results for the bearing clearance $\delta_0 = 2 \mu\text{m}$ is given in Figure 4.4.

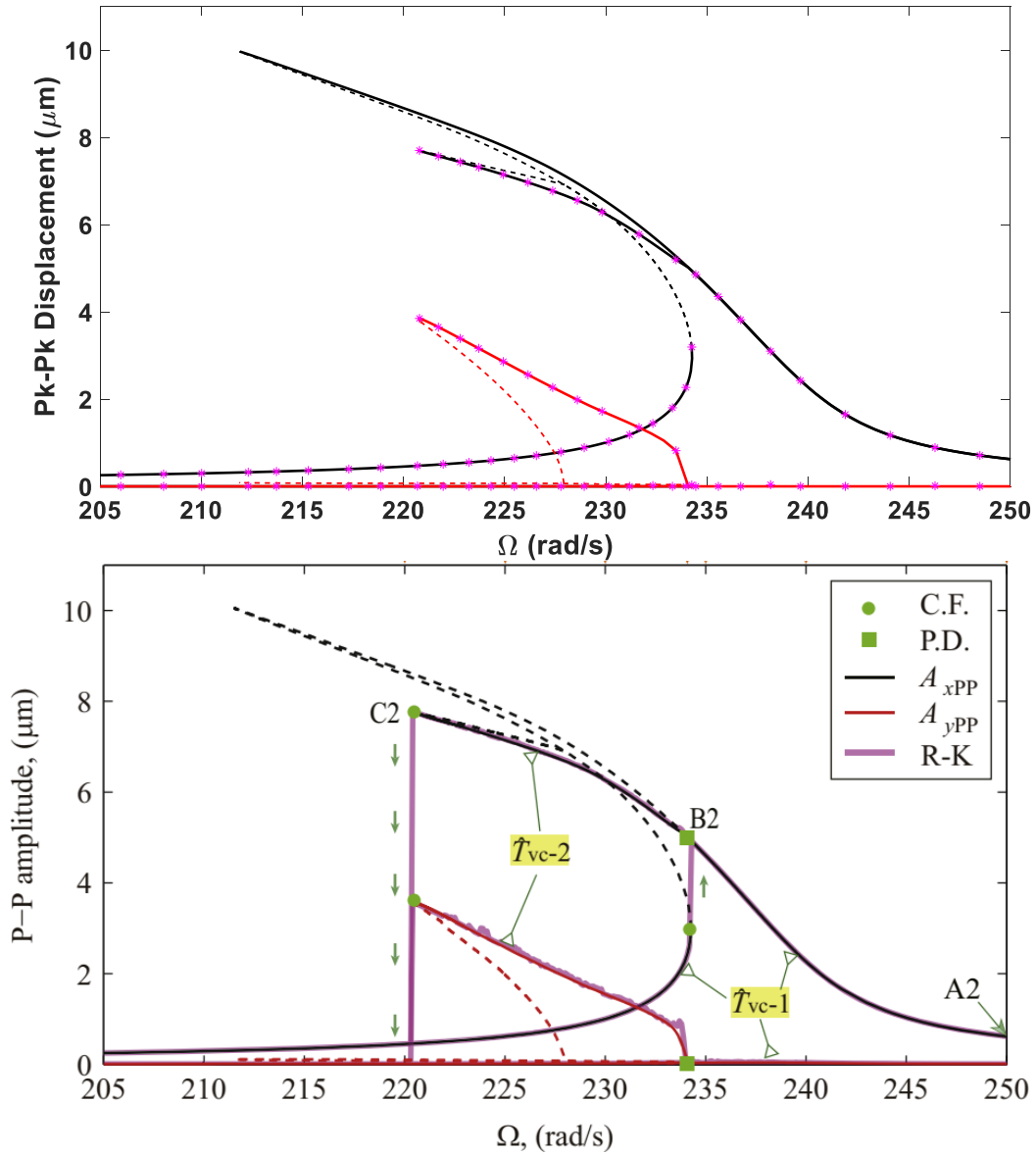


Figure 4.4. Comparison of Results for Vertical (Black) and Horizontal (Red) Directions for Varying Compliance Vibrations ($\delta_0 = 2 \mu\text{m}$)

Vibrations having the same period with varying compliance are denoted with T_{VC-1} whereas T_{VC-2} stands for oscillations having a period twice of the VC. T_{VC-1} solutions are obtained by building the Fourier series on VC frequency. On the other hand, to obtain T_{VC-2} results, base frequency for the Fourier series is $VC/2$. It is seen that, same FRFs are obtained for both cases.

In Figure 4.4, dashed lines indicate unstable periodic solutions where solid lines are for stable periodic motion. Purple FRFs in literature data and purple stars in the upper plot are obtained with Runge-Kutta integrations.

Table 4.3. Parameters for JIS6306

K_H	13.34E9 N/m ^{3/2}	D_b	11.9062 mm
N_b	8	D_p	52 mm

CHAPTER 5

CASE STUDIES

5.1. Effect of Asymmetry on Parametric Resonance

For this case study, a Jeffcott rotor geometry supported by two nonlinear ball bearings (JIS6306) is chosen. The rotor is parametrically excited, i.e., only external forcing is the weight of the rotor. Bearing internal clearance, $2\delta_0$, is taken as $10\ \mu\text{m}$. Parametric resonances are investigated by shifting disk's location closer to one of the bearings.

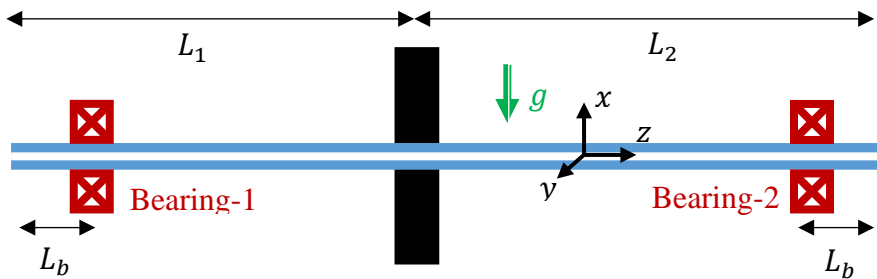


Figure 5.1. Sketch of the System for Case Study 1

Rotor geometry is shown in Figure 5.1

Table 5.1. Position of the Disk for the Configurations for Case Study 1

Configuration	L_1 (mm)	L_2 (mm)
C1 (Jeffcott)	300	300
C2	214.3	385.7

Table 5.2. Parameters for the Shaft-Disk System for Case Study 1

E	210 GPa	ν	0.3
ρ	7800 kg/m ³	η	0.01
r_i	7.5 mm	r_o	15 mm
L	600 mm	L_b	85.7 mm
r_D	160 mm	t_D	20 mm

Harmonics used for the solution are 0, 0.5 VC, VC, 2VC, 3VC and 4VC, which are observed for a balanced rotor by Fukata [9] and Tiwari [16]. Fourier series is built on 0.5VC base frequency as shown in (5.1.)

$$\mathbf{x}(t) = \mathbf{x}_0 + \sum_{p=1}^{N_H} \left(\mathbf{x}_{c,p} \cos \left(p \cdot \frac{\omega_{VC}}{2} \cdot t \right) + \mathbf{x}_{s,p} \sin \left(p \cdot \frac{\omega_{VC}}{2} \cdot t \right) \right) \quad (5.1)$$

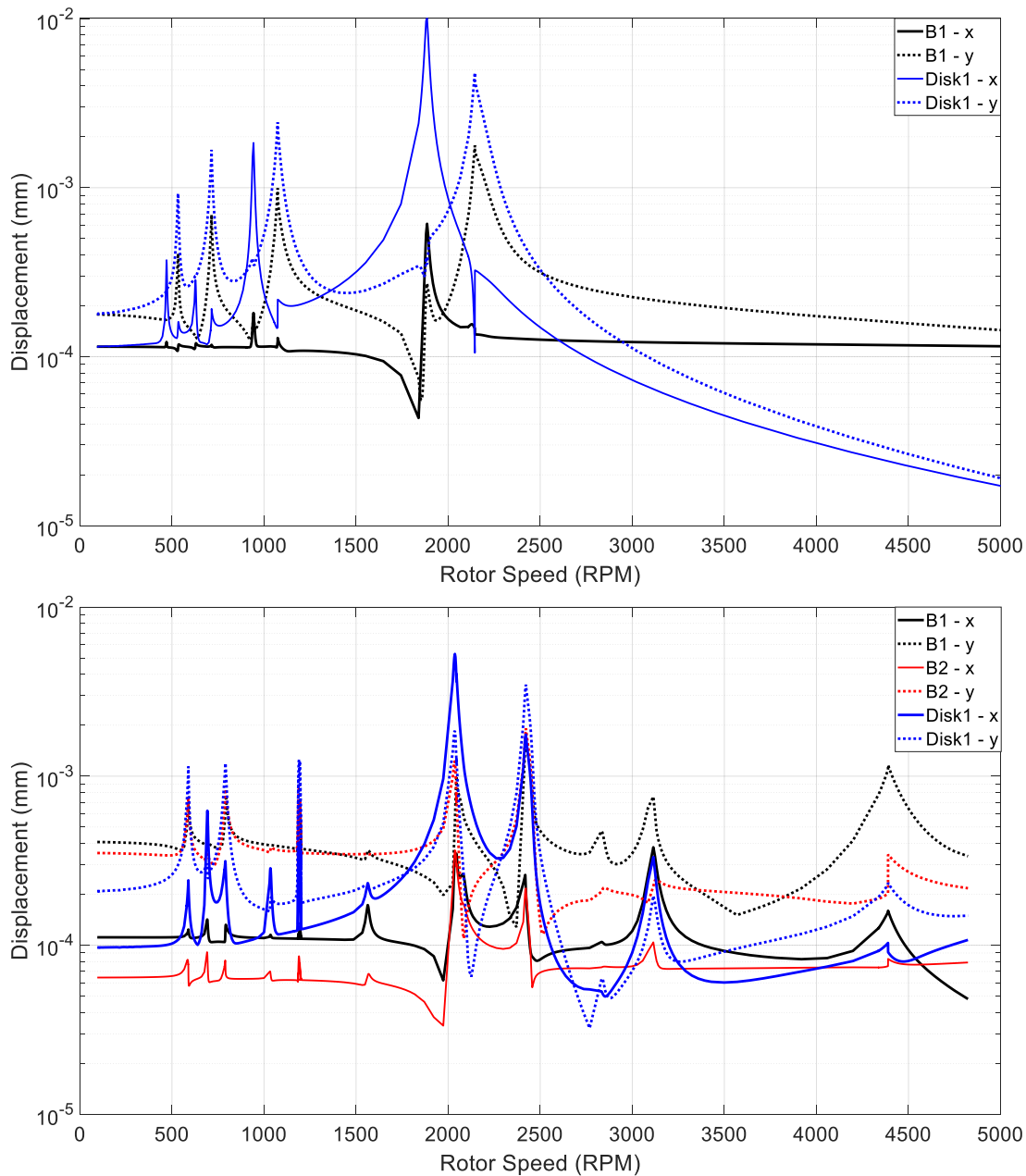


Figure 5.2. Total Responses for C1 (Upper) and C2 Configurations

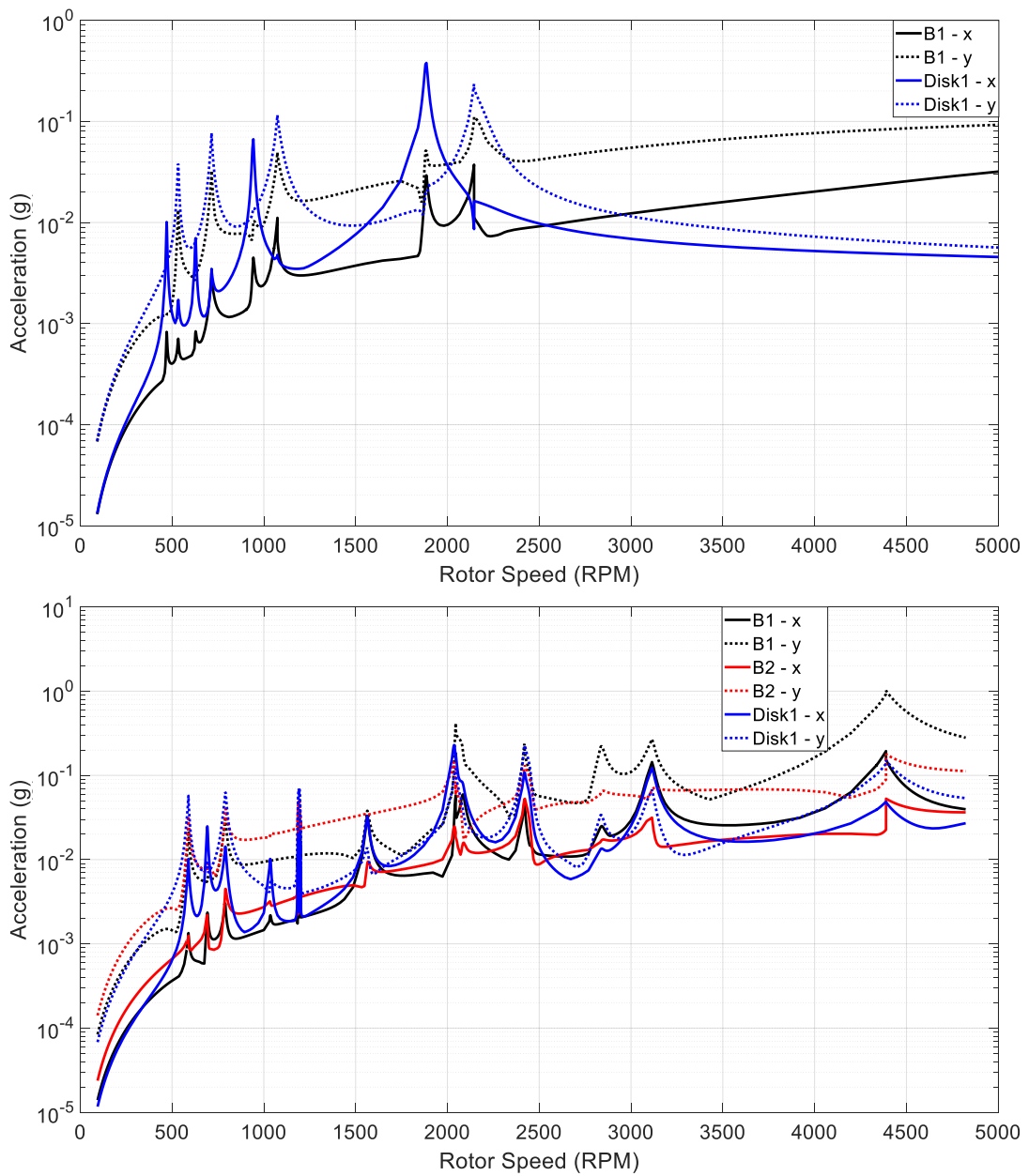


Figure 5.3. Acceleration FRFs for C1 (Upper) and C2 Configurations

As expected, Bearing-1 and 2 have the complete same responses for Jeffcott (C1) configuration so, only Bearing-1 response is plotted in Figures 5.2 and 5.3 for C1.

In Figure 5.2, it can be observed that system got stiffer as disk is moved closer to Bearing-1. Also, Bearing-1 resonances appeared around 3000 and 4500 rpm.

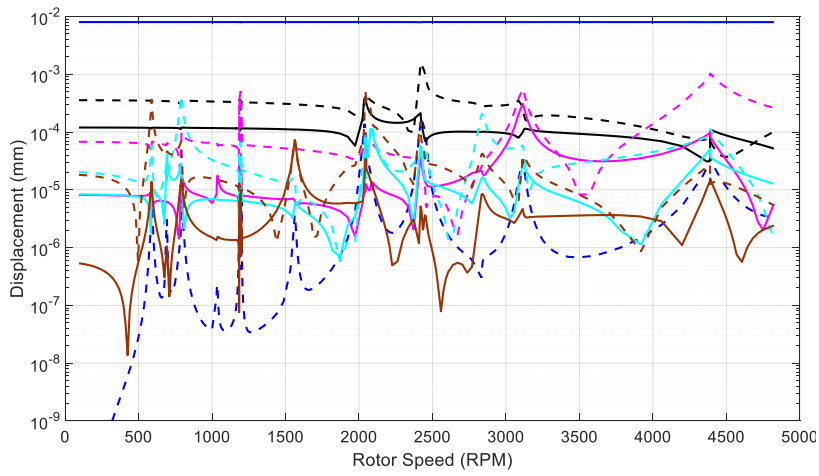
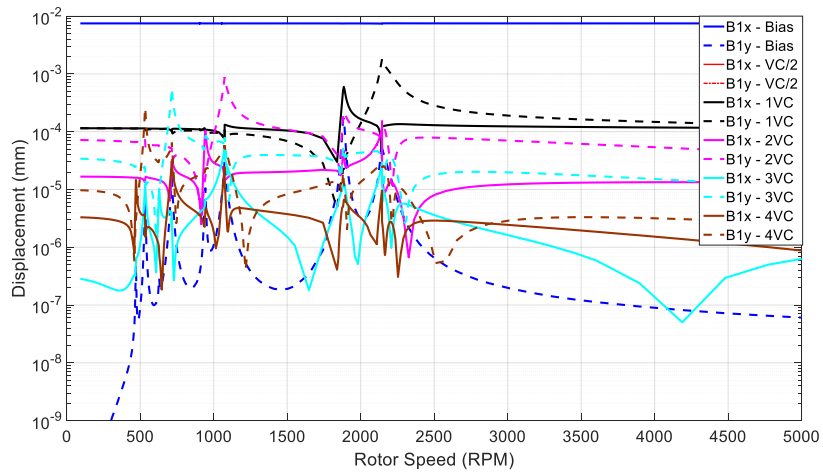


Figure 5.4. Individual Harmonic Responses for Bearing 1, C1 Top, C2 Bottom

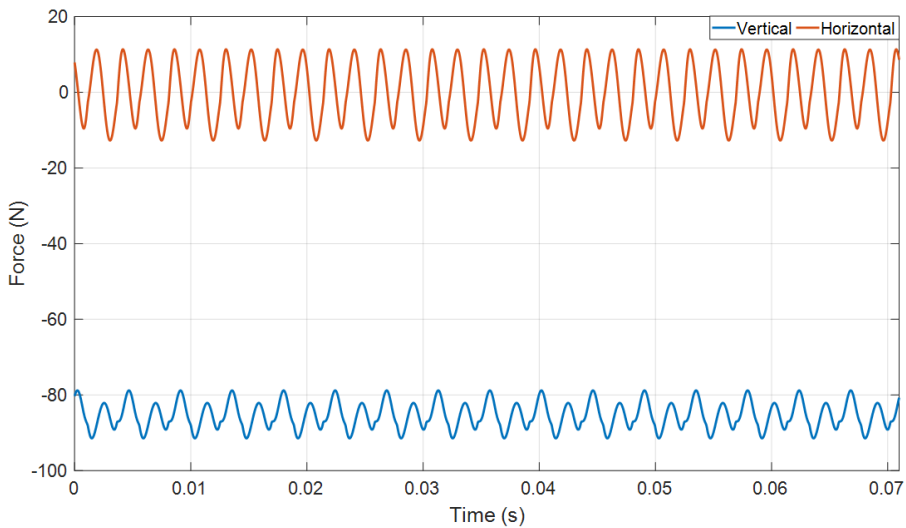


Figure 5.5. Bearing-1 Reaction Forces for C2, $\Omega = 4389$ RPM

Individual harmonic responses for Bearing-1 are provided in Figure 5.4 for C1, and C2. It can be observed that 2VC vibrations occurred as system became asymmetric. Bearing reaction forces at the resonant frequency close to 4500 rpm is given in Figure 5.5. Finally, rotor orbits are provided for resonances at 2030 and 2420 rpm for C2 in Figure 5.6. Here black and red circle denotes Bearings 1 and 2 respectively, where blue circle is for the disk.

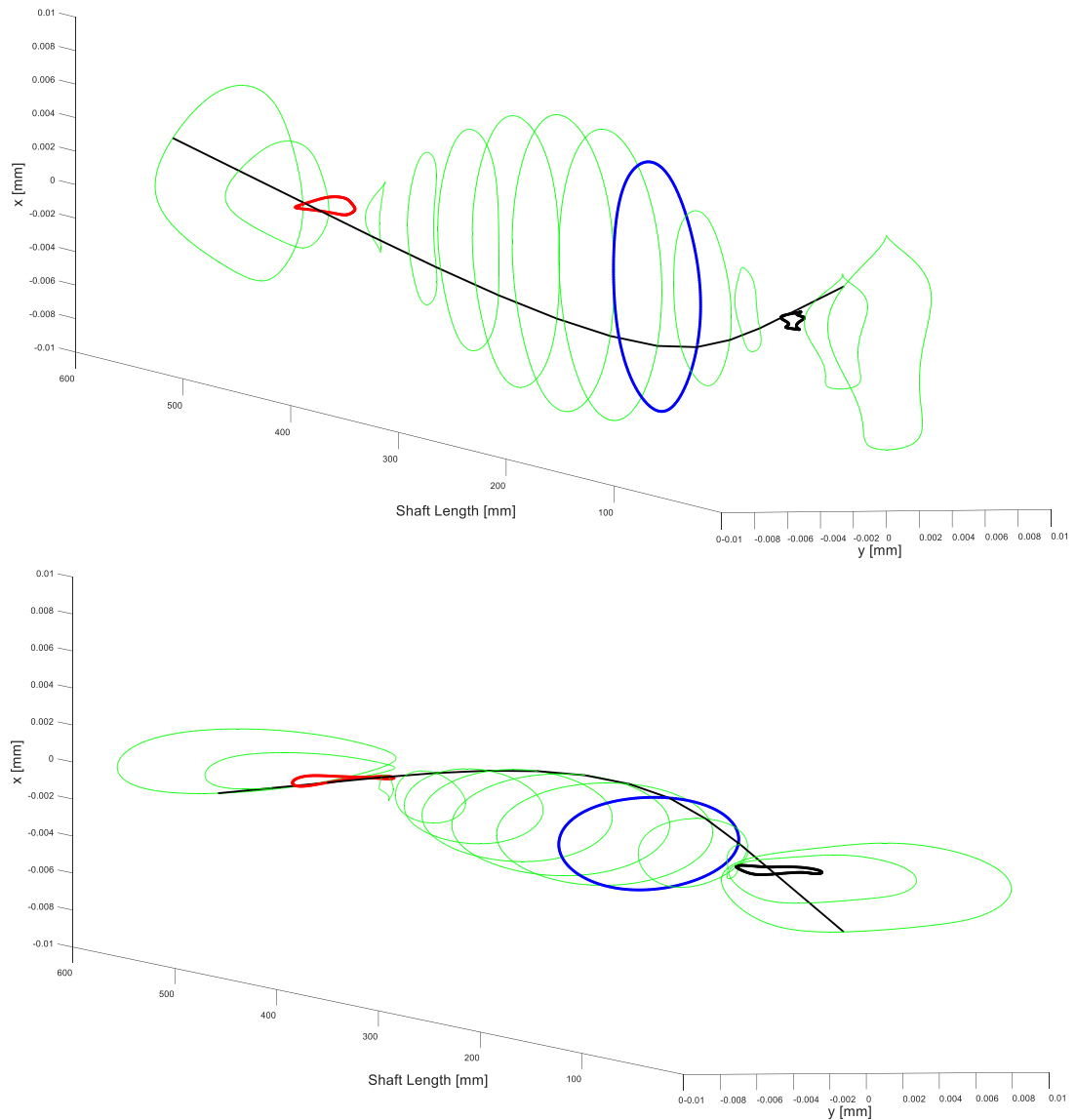


Figure 5.6. Rotor Orbits for C2 at $\Omega = 2030$ RPM Top and $\Omega = 2420$ RPM Bottom

5.2. Unbalance Response Under Multiple Excitation

For rotors carrying more than one disks, multiple unbalance excitation is always a possibility. Under such excitations, the relative angle between the unbalance forces may have a significant effect on the system response. For this case study, a rotor with two disks and supported by two nonlinear ball bearings is studied. A sketch of the system is given in Figure 5.7.

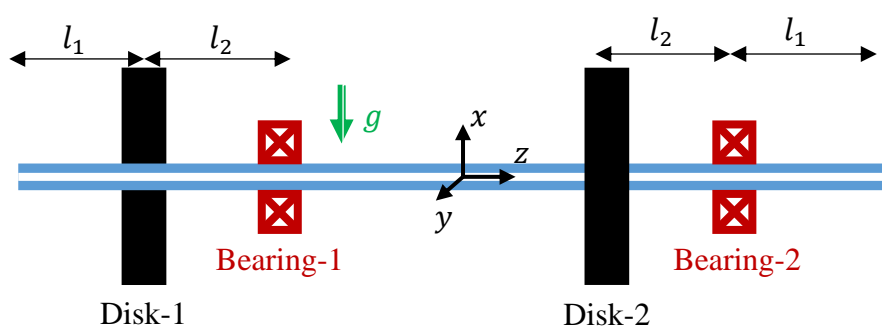


Figure 5.7. Sketch of the System for Case Study 2

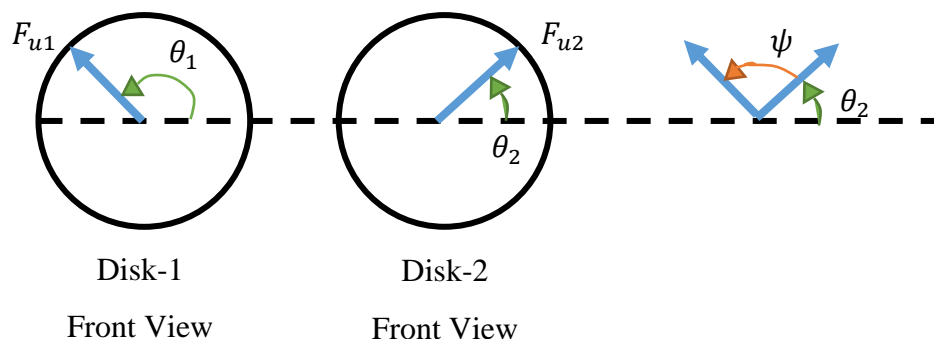


Figure 5.8. Relative Unbalance Angle, ψ

Three relative angles considered are, 0° , 90° and 180° . A sketch of concept of relative unbalance angle, ψ , is given in Figure 5.8.

Ball bearing used for this case is SKF6002. Parameters of the bearing are given in Table 5.3.

Table 5.3. Parameters for SKF6002

K_H	7.055E9 N/m^{3/2}	D_b	4.762 mm
N_b	9	D_p	24.35 mm

The ratio of cage speed to shaft speed defined by (2.3) for SKF6002 is 0.4. This allows to include harmonics coming from both rotor and the bearings into the solution. This ratio was 0.385 for JIS6306. Bearing clearance $2\delta_0$ is chosen as 7 μm , which was among the values provided by Tiwari and R&D Department of SKF for clearance class C2 [17].

Parameters for the shaft-disk system is given in Table 5.4.,

Table 5.4. Parameters for the Shaft-Disk System for Case Study 2

E	210 GPa	ν	0.3
ρ	7800 kg/m³	η	0.01
r_i	0 mm	r_o	7.5 mm
L	600 mm	l_1	85.7 mm
r_D	120 mm	l_2	128.6 mm
t_D	20 mm		

Fourier series for the solution,

$$\mathbf{x}(t) = \mathbf{x}_0 + \sum_{p=1}^{N_H} (\mathbf{x}_{c,p} \cos(p \cdot \Omega \cdot t) + \mathbf{x}_{s,p} \sin(p \cdot \Omega \cdot t)) \quad (5.2)$$

Where considered harmonics are 0, 0.5X, 1X, 2X, VC – 1X, 3X and VC + 1X, which have been observed experimentally [17]. Here nX means, n times the rotor speed Ω .

Sinou [32] has investigated unbalance response of a similar rotor structure for 2 and 4 grams of unbalance masses. For this study, an unbalance mass of 8 grams is considered. Unbalance masses are placed on the edge of the disks.

Unbalance response for three phase angles are given in Figure 5.9 and acceleration FRFs are given in Figure 5.10.

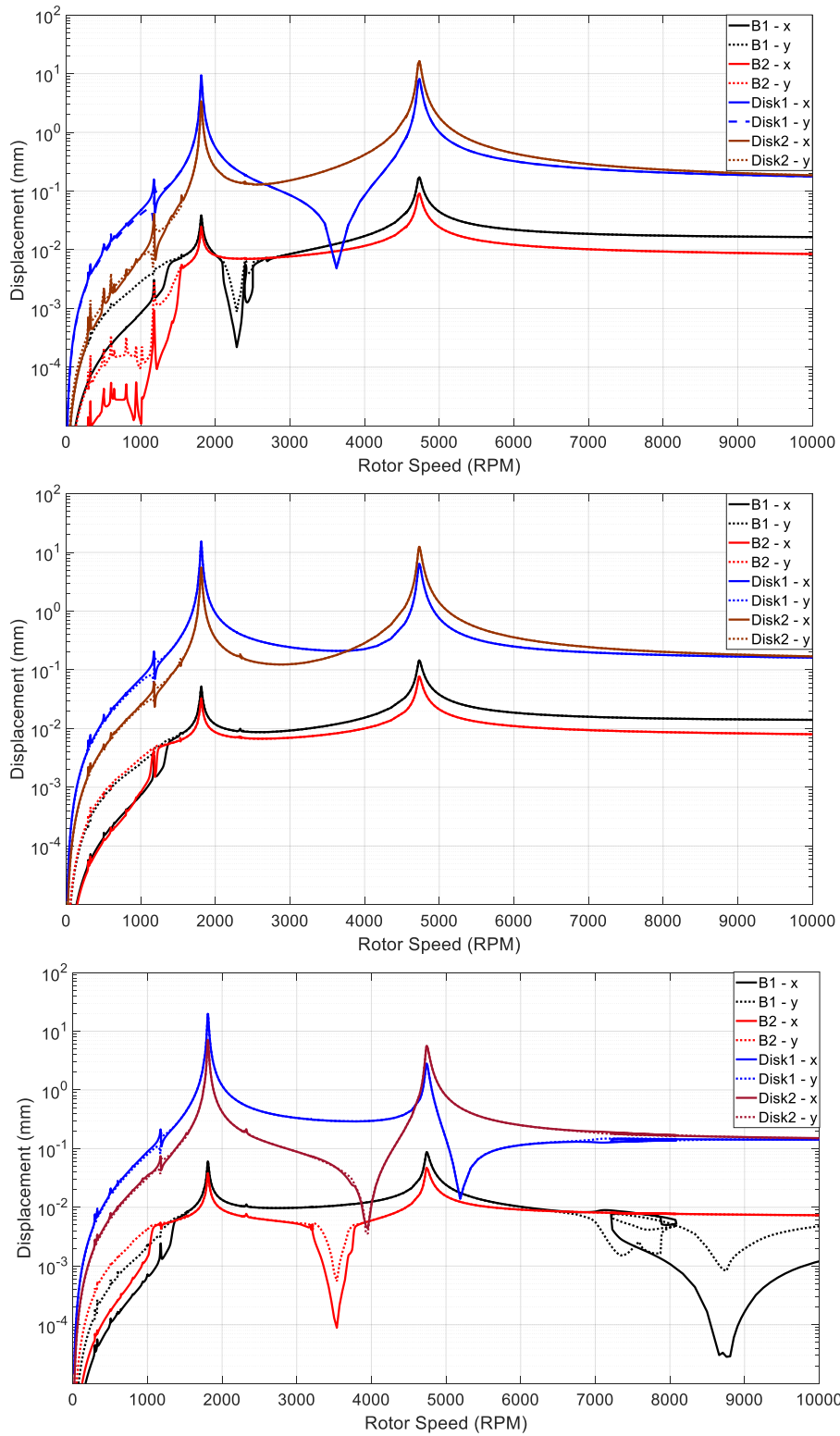


Figure 5.9. Total FRFs, Top to Bottom $\psi = 0,90,180$

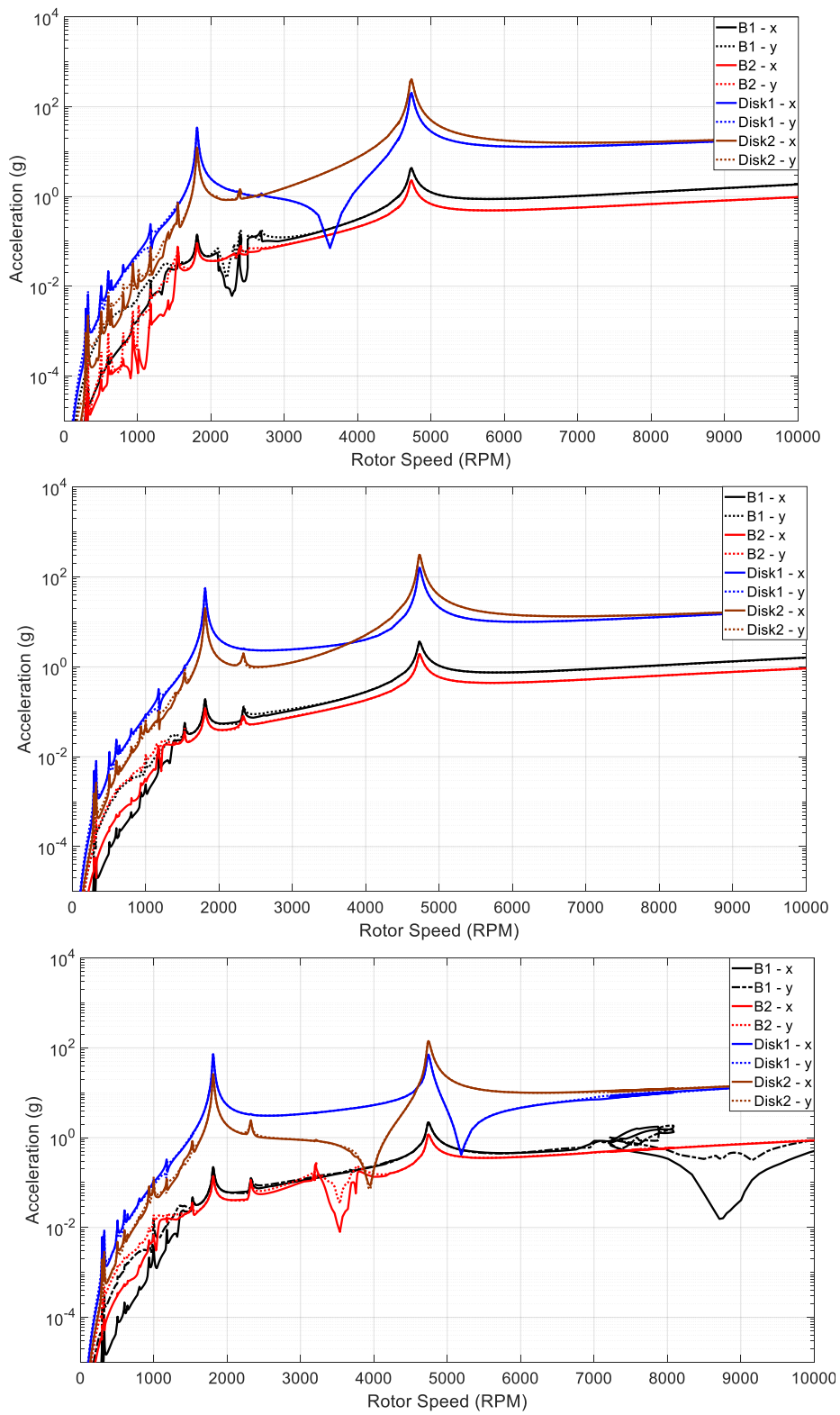


Figure 5.10. Total Acceleration FRFs, Top to Bottom $\psi = 0,90,180$

When peak points in Figure 5.9. are investigated one can notice a slight softening as ψ increases. An anti-nodal point exists for Bearing-1 for $\psi = 0^\circ$ between 2000-3000 rpm. A similar behavior is observed for Bearing-2 for $\psi = 180^\circ$ between 3000-4000 rpm. Bearing-1 has a complicated response region for $\psi = 180^\circ$ starting from 7000 rpm and continues still after 10000 rpm.

Rotor orbits for the resonances about 2000 and 5000 rpm are given in Figure 5.11. Response of each individual harmonic for both bearings are provided in Figures 5.12-5.13.

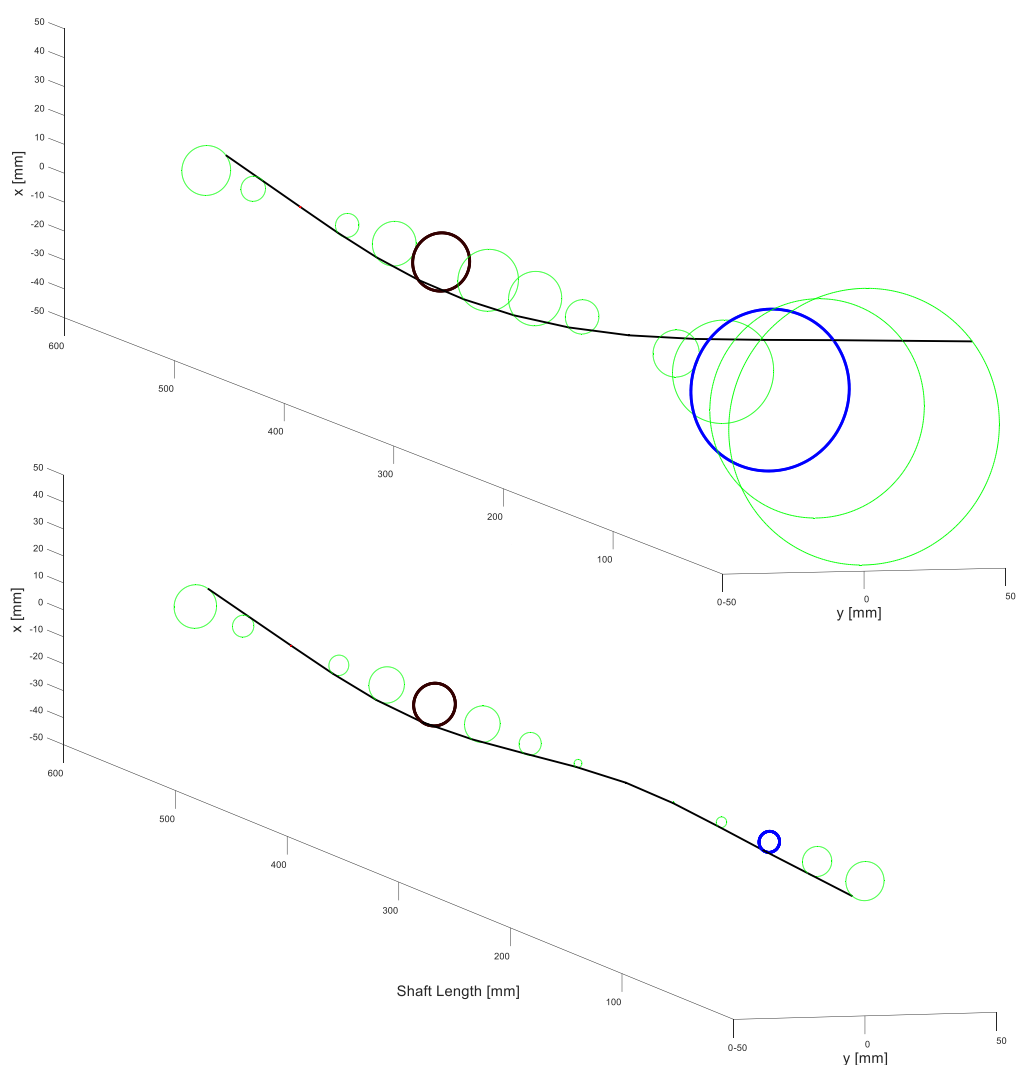


Figure 5.11. Rotor Orbits for the Resonances Around 2000 and 5000 RPM, $\psi = 180$

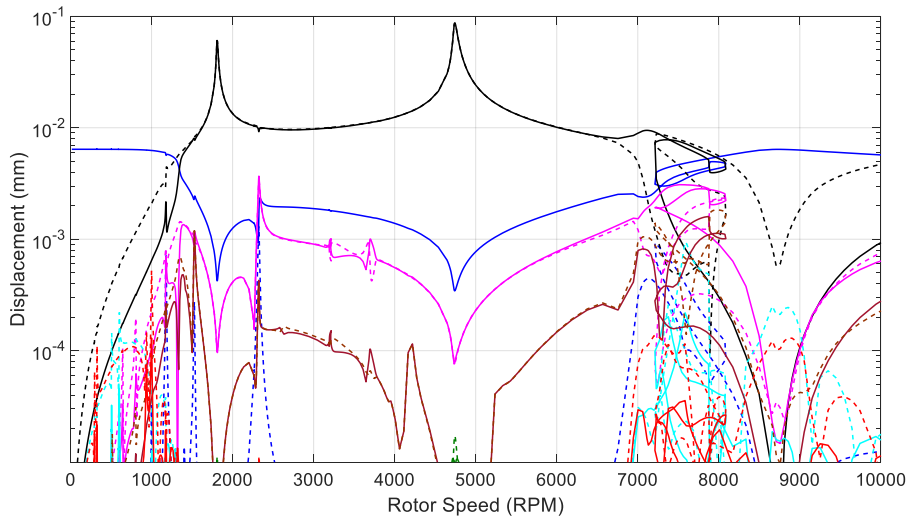
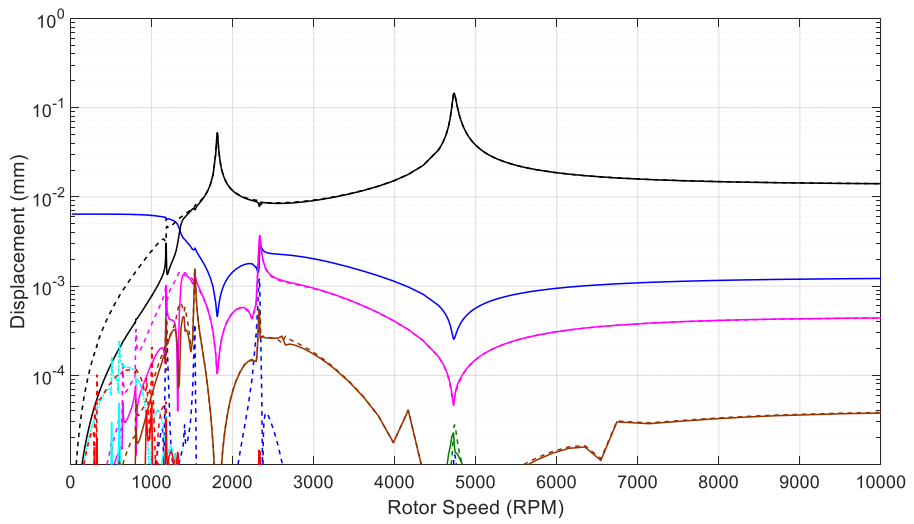
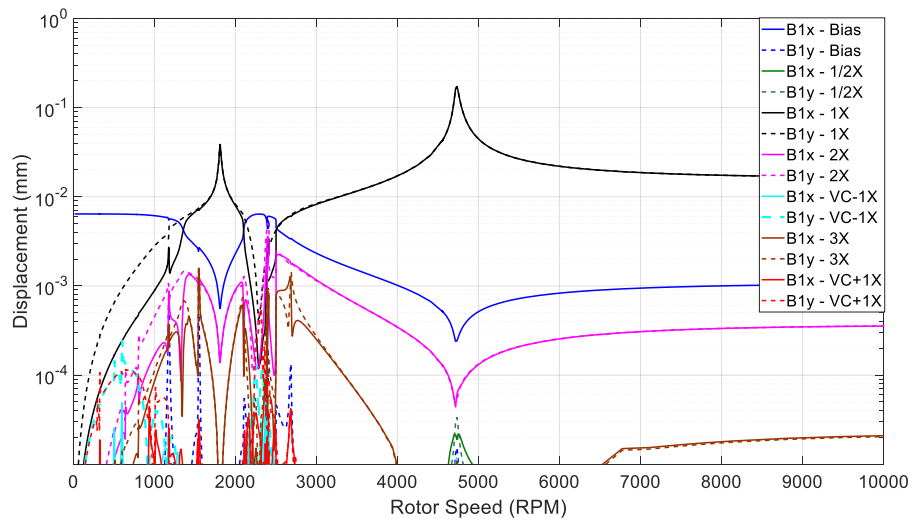


Figure 5.12. Individual Harmonics for Bearing-1, Top to Bottom $\psi = 0,90,180$

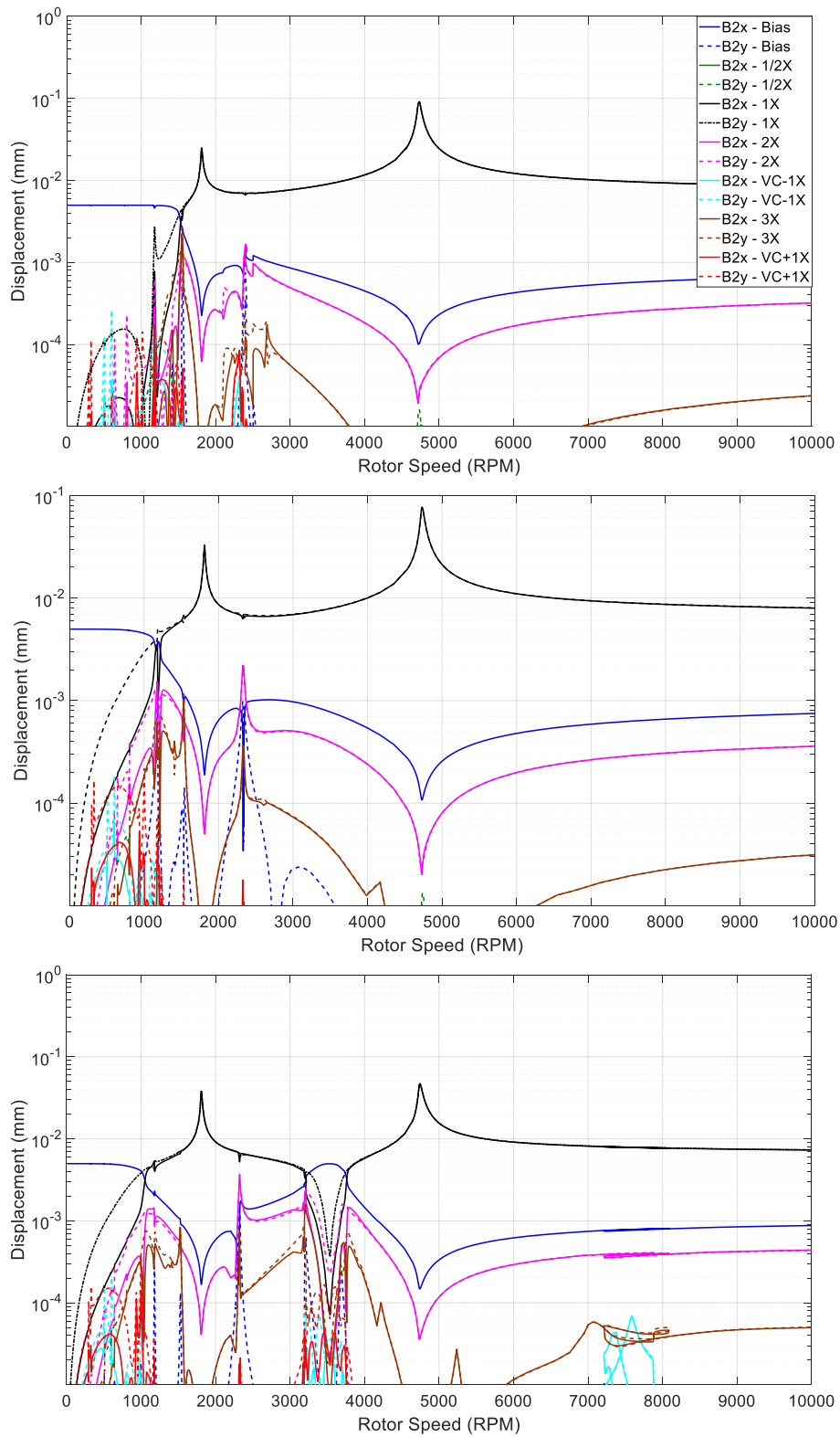


Figure 5.13. Individual Harmonics for Bearing-2, Top to Bottom $\psi = 0,90,180$

It can be seen from Figure 5.12 that amplitude of all harmonics tend to decrease for $\psi = 0^\circ$ between 2000-3000 rpm. 2X and 3X harmonics seem to have the largest amplitudes. Same conclusions can be made for $\psi = 180^\circ$ between 3000-4000 rpm. Vertical and horizontal reaction forces of the bearings are given in Figures 5.14-5.16.

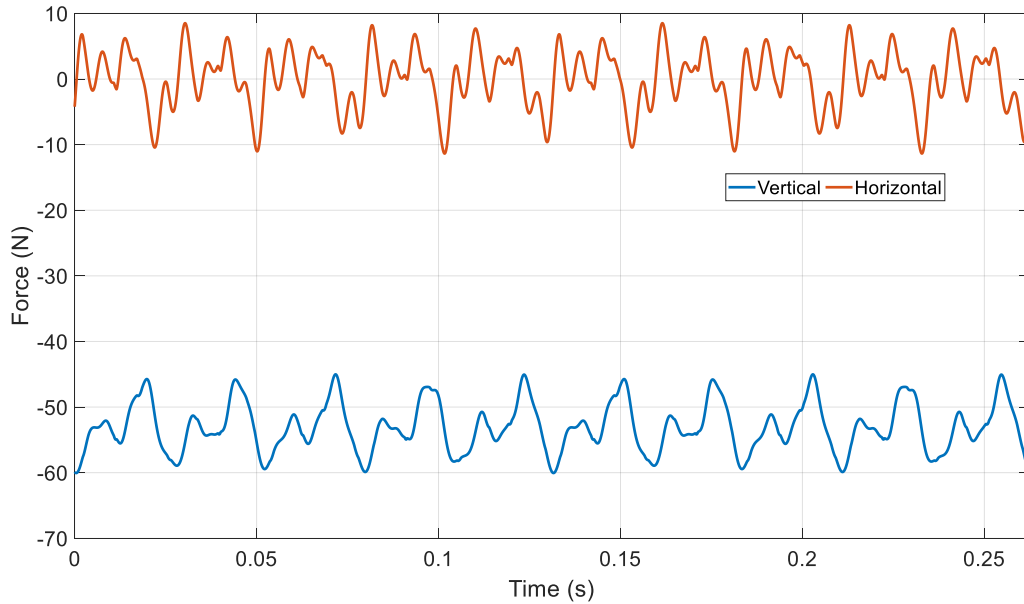


Figure 5.14. Bearing-1 Reaction Forces, $\psi = 0, \Omega = 2290$ RPM

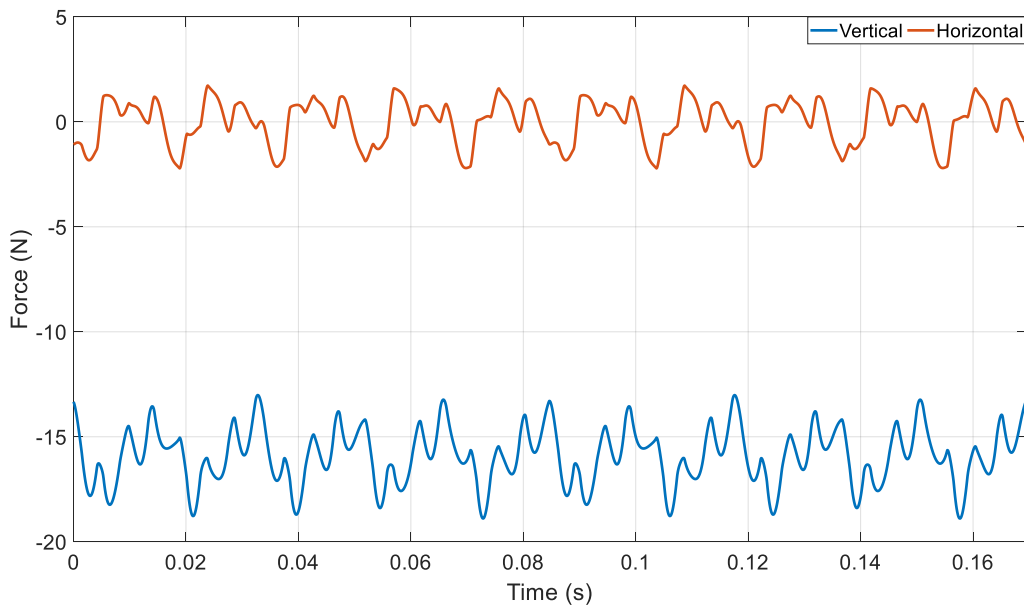


Figure 5.15. Bearing-2 Reaction Forces, $\psi = 180, \Omega = 3537$ RPM

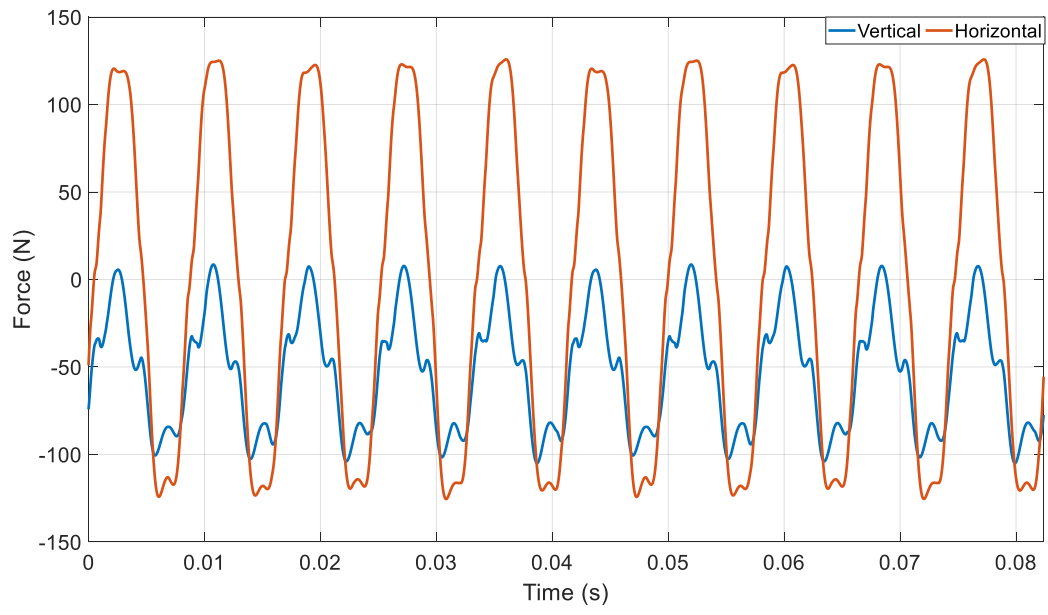


Figure 5.16. Bearing-1 Reaction Forces, $\psi = 180$, $\Omega = 7280$ RPM

CHAPTER 6

CONCLUSION

Roller Element Bearings will continue to be at the heart of the aerospace industry. Their nonlinear behavior has been a study area for almost fifty years. However, there is much to discover, especially for fast and accurate methods to help the design of complex rotor systems with these bearings. This thesis aims the development of a computer code that can model a complex rotor structure supported by any number of ball bearings and obtain solutions in the frequency domain.

For this reason, the Finite Element Method (FEM) is chosen to model different rotor geometries fast and accurately. Lumped parameter bearing model, which is widely used in the literature for bearing behavior investigation, is utilized for the bearings. Nonlinear vibration analysis in the frequency domain is accomplished by the Harmonic Balance Method. The resulting set of nonlinear algebraic equation set is then solved by Newton's Method with arclength continuation, to obtain a whole dynamic picture of the structure. Since FEM results in a large number of unknowns and few of them are nonlinear, the Receptance Method is utilized to decrease the number of nonlinear equations to be solved. REBs are generic nonlinear elements that have both clearance and Hertzian contact. Therefore, the Alternating Frequency-Time scheme is used to obtain Fourier coefficients of the unknown nonlinear forces and help the calculation of the Jacobian matrix. The stability of the solutions is checked with Hill's Method. FEM part of the computer code is tested with commercial FEM program ABAQUS. REB model is verified from the literature [61].

In Chapter 5, two case studies have been performed with the developed code. For the first case, parametric resonances of a rotor with two nonlinear ball bearings and one balanced disk have been investigated. Evaluation of the resonances and contribution of different harmonics are examined, as disk location is altered. For the second case, a similar system to the previous one but this time with two disks, under multiple

unbalance excitations have been studied. The nonlinear response is calculated for different relative unbalance angles. Orbit plots and bearing reaction forces are presented for both cases, which both can be taken as an output from the code.

REFERENCES

- [1] Cao, H., Niu, L., Xi, S., and Chen, X., 2018, “Mechanical Model Development of Rolling Bearing-Rotor Systems: A Review,” *Mech. Syst. Signal Process.*, **102**, pp. 37–58.
- [2] Oswald, F. B., Zaretsky, E. V., and Poplawski, J. V., 2011, “Interference-Fit Life Factors for Ball Bearings,” *Tribol. Trans.*, **54**(1), pp. 1–20.
- [3] Gargiulo, E. P. J., 1980, “A Simple Way to Estimate Bearing Stiffness,” *Mach. Des.*, pp. 107–110.
- [4] DyRoBeS, “DyRoBeS Manual | Rotor” [Online]. Available: <https://dyrobes.com/help1800/Rotor/html/>. [Accessed: 17-Sep-2019].
- [5] Tamura, H., Gad, E. H., and Kondoui, T., 1985, “On the Static Running Accuracy of Ball Bearings,” *Bull. JSME*, **28**, pp. 1240–1246.
- [6] Leader, M. E., “A Practical Guide to Rotor Dynamics.”
- [7] Childs, D. W., and Moyer, D. S., 1985, “Vibration Characteristics of the HPOTP (High-Pressure Oxygen Turbopump) of the SSME (Space Shuttle Main Engine),” *J. Eng. Gas Turbines Power*, **107**(1), p. 152.
- [8] Sunnersjö, C. S., 1978, “Varying Compliance Vibrations of Rolling Bearings,” *J. Sound Vib.*, **58**(3), pp. 363–373.
- [9] Fukata, S., Gad, E. H., Kondoui, T., Ayabe, T., and H, T., 1985, “On the Radial Vibration of Ball Bearings,” *JSPM*, **28**(239), pp. 899–904.
- [10] Saito, S., 1985, “Calculation of Nonlinear Unbalance Response of Horizontal Jeffcott Rotors Supported by Ball Bearings With Radial Clearances,” *J. Vib. Acoust. Stress Reliab. Des.*, **107**(4), p. 416.
- [11] Kim, Y. B., and Noah, S. T., 1990, “Bifurcation Analysis for a Modified Jeffcott Rotor with Bearing Clearances,” *Nonlinear Dyn.*, **1**(3), pp. 221–241.
- [12] Kim, Y. B., and Noah, S. T., 1996, “Quasi-Periodic Response and Stability Analysis for a Non-Linear Jeffcott Rotor,” *J. Sound Vib.*, **190**(2), pp. 239–253.
- [13] Ehrich, F., 1992, “Observations of Subcritical Superharmonic and Chaotic Response in Rotordynamics,” *J. Vib. Acoust.*, **114**(1), p. 93.
- [14] B.Mevel and J.L.Guyader, 1993, “Routes to Chaos in Ball Bearings,” pp. 471–487.
- [15] Tiwari, M., Gupta, K., and Prakash, O., 2000, “Dynamic Response of an Unbalanced Rotor Supported on Ball Bearings,” *J. Sound Vib.*, **238**(5), pp.

757–779.

- [16] Tiwari, M., Gupta, K., and Prakash, O., 2000, “Effect of Radial Internal Clearance of a Ball Bearing on the Dynamics of a Balanced Horizontal Rotor,” *J. Sound Vib.*, **238**(5), pp. 723–756.
- [17] Tiwari, M., Gupta, K., and Prakash, O., 2002, “Experimental Study of a Rotor Supported by Deep Groove Ball Bearing,” *Int. J. Rotating Mach.*, **8**(4), pp. 243–258.
- [18] Harsha, S. P., Sandeep, K., and Prakash, R., 2003, “The Effect of Speed of Balanced Rotor on Nonlinear Vibrations Associated with Ball Bearings,” *Int. J. Mech. Sci.*, **45**(4), pp. 725–740.
- [19] Harsha, S. P., 2005, “Non-Linear Dynamic Response of a Balanced Rotor Supported on Rolling Element Bearings,” **19**, pp. 551–578.
- [20] Lioulios, A. N., and Antoniadis, I. A., 2006, “Effect of Rotational Speed Fluctuations on the Dynamic Behaviour of Rolling Element Bearings with Radial Clearances,” *Int. J. Mech. Sci.*, **48**(8), pp. 809–829.
- [21] Villa, C. V. S., Sinou, J.-J., and Thouverez, F., 2007, “Investigation of a Rotor-Bearing System with Bearing Clearances and Hertz Contact by Using a Harmonic Balance Method,” *J. Brazilian Soc. Mech. Sci. Eng.*, **29**(1), pp. 14–20.
- [22] Bai, C., Zhang, H., and Xu, Q., 2008, “Effects of Axial Preload of Ball Bearing on the Nonlinear Dynamic Characteristics of a Rotor-Bearing System,” *Nonlinear Dyn.*, **53**(3), pp. 173–190.
- [23] Cheng, M., Meng, G., and Wu, B., 2012, “Nonlinear Dynamics of a Rotor-Ball Bearing System with Alford Force,” *JVC/Journal Vib. Control*, **18**(1), pp. 17–27.
- [24] Bai, C., Zhang, H., and Xu, Q., 2013, “Subharmonic Resonance of a Symmetric Ball Bearing-Rotor System,” *Int. J. Non. Linear. Mech.*, **50**, pp. 1–10.
- [25] Zhang, X., Han, Q., Peng, Z., and Chu, F., 2013, “Stability Analysis of a Rotor-Bearing System with Time-Varying Bearing Stiffness Due to Finite Number of Balls and Unbalanced Force,” *J. Sound Vib.*, **332**(25), pp. 6768–6784.
- [26] Zhang, X., Han, Q., Peng, Z., and Chu, F., 2015, “A New Nonlinear Dynamic Model of the Rotor-Bearing System Considering Preload and Varying Contact Angle of the Bearing,” *Commun. Nonlinear Sci. Numer. Simul.*, **22**(1–3), pp. 821–841.
- [27] Hou, L., Chen, Y., Fu, Y., Chen, H., Lu, Z., and Liu, Z., 2017, “Application of the HB–AFT Method to the Primary Resonance Analysis of a Dual-Rotor System,” *Nonlinear Dyn.*, **88**(4), pp. 2531–2551.

- [28] Wang, H., Han, Q., and Zhou, D., 2017, “Nonlinear Dynamic Modeling of Rotor System Supported by Angular Contact Ball Bearings,” *Mech. Syst. Signal Process.*, **85**, pp. 16–40.
- [29] Jin, Y., Yang, R., Hou, L., Chen, Y., and Zhang, Z., 2017, “Experiments and Numerical Results for Varying Compliance Contact Resonance in a Rigid Rotor–Ball Bearing System,” *J. Tribol.*, **139**(4), p. 041103.
- [30] Yang R, Hou L, Jin Y, Chen Y, Z. Z., 2018, “The Varying Compliance Resonance in a Ball Bearing Rotor System Affected by Different Ball Numbers and Rotor Eccentricities,” *ASME. J. Tribol*, **140**(September), pp. 1–10.
- [31] Villa, C., Sinou, J. J., and Thouverez, F., 2008, “Stability and Vibration Analysis of a Complex Flexible Rotor Bearing System,” *Commun. Nonlinear Sci. Numer. Simul.*, **13**(4), pp. 804–821.
- [32] Sinou, J. J., 2009, “Non-Linear Dynamics and Contacts of an Unbalanced Flexible Rotor Supported on Ball Bearings,” *Mech. Mach. Theory*, **44**(9), pp. 1713–1732.
- [33] Gupta, T. C., Gupta, K., and Sehgal, D. K., 2010, “Instability and Chaos of a Flexible Rotor Ball Bearing System: An Investigation on the Influence of Rotating Imbalance and Bearing Clearance,” *ASME Turbo Expo 2010: Power for Land, Sea and Air*.
- [34] Babu, C. K., Tandon, N., and Pandey, R. K., 2014, “Nonlinear Vibration Analysis of an Elastic Rotor Supported on Angular Contact Ball Bearings Considering Six Degrees of Freedom and Waviness on Balls and Races,” *J. Vib. Acoust.*, **136**(4), p. 044503.
- [35] Yi, J., Liu, H., Wang, F., Li, M., and Jing, M., 2014, “The Resonance Effect Induced by the Variable Compliance Vibration for an Elastic Rotor Supported by Roller Bearings,” *Proc. Inst. Mech. Eng. Part K J. Multi-body Dyn.*, **228**(4), pp. 380–387.
- [36] Li, Y., Cao, H., Niu, L., and Jin, X., 2015, “A General Method for the Dynamic Modeling of Ball Bearing–Rotor Systems,” *J. Manuf. Sci. Eng.*, **137**(2), p. 021016.
- [37] Metsebo, J., Upadhyay, N., Kankar, P. K., and Nana Nbandjo, B. R., 2016, “Modelling of a Rotor-Ball Bearings System Using Timoshenko Beam and Effects of Rotating Shaft on Their Dynamics,” *J. Mech. Sci. Technol.*, **30**(12), pp. 5339–5350.
- [38] Lu, Z., Wang, X., Hou, L., Chen, Y., and Liu, X., 2019, “Nonlinear Response Analysis for an Aero Engine Dual-Rotor System Coupled by the Inter-Shaft Bearing,” *Arch. Appl. Mech.*, **89**(7), pp. 1275–1288.
- [39] Friswell, M. I., Penny, J. E. T., Garvey, S. D., and Lees, A. W., 2010,

- “Dynamics of Rotating Machines (Cambridge Aerospace Series).”
- [40] Nelson, H. D., and McVaugh, J. M., 1976, “The Dynamics of Rotor-Bearing Systems Using Finite Elements,” *J. Eng. Ind.*, **98**(2), p. 593.
 - [41] Chen, W. J., *Practical Rotordynamics and Fluid Film Bearing Design*.
 - [42] Nassis, A., 2010, “Analyses of a Rotor Dynamic Testrigs,” Luea University.
 - [43] Harris, T. A., *Rolling Bearing Analysis*.
 - [44] Krack, M., and Gross, J., 2019, *Harmonic Balance for Nonlinear Vibration Problems*, Springer.
 - [45] Cochelin, B., and Vergez, C., 2009, “A High Order Purely Frequency-Based Harmonic Balance Formulation for Continuation of Periodic Solutions,” *J. Sound Vib.*, **324**(1–2), pp. 243–262.
 - [46] Legrand, M., Roques, S., Pierre, C., Peseux, B., and Cartraud, P., 2007, “N-Dimensional Harmonic Balance Method Extended to Non-Explicit Nonlinearities,” *Eur. J. Comput. Mech.*, **15**(1–3), pp. 269–280.
 - [47] Guskov, M., Sinou, J. J., and Thouverez, F., 2008, “Multi-Dimensional Harmonic Balance Applied to Rotor Dynamics,” *Mech. Res. Commun.*, **35**(8), pp. 537–545.
 - [48] Junge, L., Ashcroft, G., Kersken, H.-P., and Frey, C., 2018, “On the Development of Harmonic Balance Methods for Multiple Fundamental Frequencies,” p. V02CT42A012.
 - [49] Cameron, T. M., and Griffin, J. H., 1989, “An Alternating Frequency/Time Domain Method for Calculating the Steady-State Response of Nonlinear Dynamic Systems,” *J. Appl. Mech.*, **56**(1), p. 149.
 - [50] FE-SAFE, “Signal Processing Reference Guide.”
 - [51] Menq, C. H., and Griffin, J. H., 1985, “A Comparison of Transient and Steady State Finite Element Analyses of the Forced Response of a Frictionally Damped Beam,” *J. Vib. Acoust. Trans. ASME*, **107**(1), pp. 19–25.
 - [52] Menq, C.-H., Griffin, J. H., and Bielak, J., 1986, “The Forced Response of Shrouded Fan Stages,” **108**(January 1986), pp. 50–55.
 - [53] Yavuz, S. D., Saribay, Z. B., and Cigeroglu, E., 2018, “Nonlinear Time-Varying Dynamic Analysis of a Spiral Bevel Geared System,” *Nonlinear Dyn.*, **92**(4), pp. 1901–1919.
 - [54] Von Groll, G., and Ewins, D. J., 2001, “ARC-LENGTH CONTINUATION IN ROTOR / STATOR CONTACT PROBLEMS,” **241**, pp. 223–233.
 - [55] Yümer, M. E., Ciğeroğlu, E., and Özgüven, H. N., 2011, “Non-Linear Forced

Response Analysis of Mistuned Bladed Disk Assemblies,” pp. 757–766.

- [56] Cigeroglu, E., and Samandari, H., 2012, “Nonlinear Free Vibration of Double Walled Carbon Nanotubes by Using Describing Function Method with Multiple Trial Functions,” *Phys. E Low-dimensional Syst. Nanostructures*, **46**, pp. 160–173.
- [57] Vasilios, N., *Nonlinear Analysis of Structures: The Arclength Method*.
- [58] Ruiz, D., 2001, “A Scaling Algorithm to Equilibrate Both Rows and Columns Norms in Matrices,” *Inst. Natl. Polytech. Toulouse Toulouse*, (RT/APO/01/4), pp. 1–21.
- [59] Xie, L., Baguet, S., Prabel, B., and Dufour, R., 2017, “Bifurcation Tracking by Harmonic Balance Method for Performance Tuning of Nonlinear Dynamical Systems,” *Mech. Syst. Signal Process.*, **88**(November 2016), pp. 445–461.
- [60] Lazarus, A., and Thomas, O., 2010, “Une Méthode Fréquentielle Pour Le Calcul de Stabilité Des Solutions Périodiques Des Systèmes Dynamiques,” *Comptes Rendus - Mec.*, **338**(9), pp. 510–517.
- [61] Zhang, Z., Chen, Y., and Cao, Q., 2015, “Bifurcations and Hysteresis of Varying Compliance Vibrations in the Primary Parametric Resonance for a Ball Bearing,” *J. Sound Vib.*, **350**, pp. 171–184.